SPE 167711

Numerical Simulation of Low Permeability Unconventional Gas Reservoirs

Didier Yu Ding[1], Yu-Shu Wu[2], Nicolas Farah[1], Cong Wang[2] and Bernard Bourbiaux[1],
[1] IFP Energies nouvelles, [2] Colorado School of Mines

This paper was prepared for presentation at the SPE/EAGE European Unconventional Conference and Exhibition held in Vienna, Austria, 25–27 February 2014.

Abstract

Unconventional gas resources from tight sand and shale gas reservoirs have received great attention in the past decade and become the focus of the petroleum industry as well as energy resources worldwide, because of their large reserves as well as technical advances in developing unconventional resources. Compared to conventional reservoirs, gas production in ultra-low-permeability unconventional reservoirs is driven by highly non-linear flow equations and involves many coexisting processes due to the presence of multi-scale fracture networks, and to the heterogeneous nature of a porous/fractured and stress-sensitive rock. Therefore, quantifying flow in unconventional gas reservoirs remains a significant challenge.

In this paper, we discuss a mathematical model and a numerical approach for simulating the production of unconventional gas reservoirs, in order to assess well performance and understand the critical parameters that affect gas recovery. Specifically, we consider the flow behavior in a stimulated reservoir volume (SRV) including a tight matrix and multi-scale fracture networks, namely primary hydraulic fractures, induced secondary fractures and micro-fractures. The feasibility and the limits in the use of single-porosity or dual-porosity reservoir models to simulate gas flow in such a system are discussed, and a multi-porosity approach is evaluated. The impacts of various physics related to unconventional gas reservoirs, such as adsorption/desorption, Klinkenberg and geomechanical effects, are quantified.

This work helps to improve simulation technologies for low-permeability unconventional gas reservoirs. An appropriate modeling approach actually underlies effective simulation tools for quantitative studies of unconventional reservoir dynamics and performance, taking into account multi-scale fracture impacts on gas production, well and stimulation design, and optimal production schedules in field development.

Introduction

Unconventional tight-gas or shale-gas reservoirs require stimulation via hydraulic fracturing to create fracture networks for practical exploitation. Within a stimulated reservoir volume (SRV), gas flows from the nano-Darcy scale to the complex fracture network and then to the well for production. The reservoir dynamics is characterized by highly non-linear behavior coupled by many co-existing process, such as gas desorption, Klinkenberg effect, non-Darcy flow, and rock deformation, in extremely low permeability reservoirs.

Many studies and progresses have been made for unconventional reservoir resources since last decade (see, for example, Wang, 2009; King, 2010; Andrade, 2010, Leahy-Dios, et al. 2011, Darishchev et al. 2013). Blasingame (2008) and Moridis et al. (2010) provide very comprehensive review of flow mechanisms in unconventional shale gas reservoirs. Many authors use directly commercial reservoir simulators to study the gas production from a shale gas reservoir or in an integrate workflow (see, for example, Cipolla et al. 2009b; Cipolla et al. 2010; Rubin 2010; Mirzaei and Cipolla, 2012). However, our understanding of gas flow and effective tools for the development of unconventional reservoirs is still far behind the industry needs. Previously, Wu et al. (2011, 2012, 2013) have presented a generalized framework model to integrate various physics involved in flow simulations in extremely low permeability fractured reservoirs. Based on that integrated framework model,

the present paper identifies the most critical physics and parameters to be considered in shale-gas flow modeling for the development of simulation tools that are adapted to unconventional reservoirs. We will also discuss simulation techniques for practical applications.

Contrary to the conventional reservoirs, the key success in a shale-gas reservoir is to focus on the well scale rather than on the field scale. Wells are hydraulically fractured to get economical gas production. To be able to evaluate correctly the well performance, it is important to properly model hydraulic fractures and predict the flow in the reservoir. In the numerical examples, we will focus our studies on the well production simulation around a single fracture or in a SRV.

Gas desorption has proved to be essential to understanding the production capacity of shale gas reservoir (see, for example, Passey et al., 2010). This is because shales can hold significant quantities of gas adsorbed on the surface of the organics (and clays) in shale formations (Mengal and Wattenbarger, 2011). In shales, methane molecules are adsorbed mainly on the carbon-rich components, *i.e.* kerogen, which are usually quantified in terms of Total Organic Carbon (TOC). As the pressure decreases with continuous gas production from reservoirs, more adsorbed gas is released from solid to free gas phase, contributing to flow and production.

Geomechanics plays a critical role in gas production and development from unconventional resources. This is because fracture properties, the most important flow parameter for gas production, are very sensitive to change in stress in shale gas reservoirs. Shale gas production depends on fractures, i.e., hydraulic fractures, induced secondary fractures, and micro fractures, if present. In addition, because of the low permeability of unconventional reservoirs, to achieve reasonable gas production rates needs to significantly lower well bottom-hole pressure to maximize pressure drops between well and reservoir to mobilize more gas to the well. This will creates a large change in pressure field, leading to a large change in effective stress, which may cause large rock deformation. As a result, the aperture and permeability of micro channels and fractures are altered. In general, rock deformation has a significant impact on both fracture and matrix permeability in a shale-gas reservoir. Bustin et al. (2008) report such geomechanical effects for Barnett, Muskwa, Ohio, and Woodford shales and show that the degree of permeability reduction due to pressure drop is significantly higher in shales than that in consolidated sandstones or carbonates. Wang et al. (2009) show that permeability in the Marcellus Shale is pressure dependent and decreases with an increase in confining of pore pressure (or total stress). Cipolla et al. (2009a) summarize some laboratory studiesregarding the conductivity of partially propped and unpropped fractures as a function of closure stress. When the reservoir is depleted, both fracture and matrix permeabilities are decreased, and gas production may be significantly reduced.

Because of complicated flow behavior, strong interaction between fluid and rock as well as multi-scaled heterogeneity, the traditional Darcy-law-based model may not be in general applicable for describing flow phenomena in unconventional gas reservoirs. Blasingame (2008) points out that high-velocity may turn out to be important in shale gas production, as gas flows mainly in the fractures towards the well. The gas velocity might be particularly large in the region close to the well. The *Forchheimer* equation is probably sufficient to represent the high-velocity of gas flow in shale gas reservoirs for many applications.

The Klinkenberg (1941) or gas-slippage effect, which has been practically ignored in conventional gas reservoir studies, is expected to be significant in shale gas reservoirs, because of the small or nanopores of shales. Soeder (1988) and Wang et al. (2009) show that gas permeability in the Marcellus Shale increases from 19.6 μD at 1,000 psi to 54 μD at 80 psi, because of the Klinkenberg effect. The study of Sakhaee-Pour and Bryant (2011), which investigates the effect of declining field pressure on the gas permeability using the network model, concludes also that the gas permeability of shale is highly dependent on the pressure due to slippage effect.

On the basis of the generalized framework model (Wu et al., 2011, 2012, 2013) and using PumaFlow simulator (PumaFlow, 2012), this paper assesses the respective impacts of the different physical phenomena discussed above and identify critical parameters for the flow dynamics in shale-gas reservoirs.

Complex fracture networks, including primary hydraulic fractures, induced secondary fractures which are generally perpendicular to the primary hydraulic fractures, and also natural macro- or micro-fractures, are usually considered in a shale-gas reservoir. In our simulations, the hydraulic fracture and induced secondary fractures are explicitly discretized in a single-porosity model. Alternatively, a dual-porosity model can be used to simulate flows in these hydraulic and induced secondary fractures on a specific "fracture" grid that exchanges fluids with another "matrix" grid. If natural fractures are presented, their petrophysical properties such as porosity and permeability are homogenized together with those of the matrix medium in matrix cells (in both single- and dual-porosity models) that hence represent the naturally-fractured matrix medium as a whole.

One of the critical issues in numerical modeling for shale gas reservoirs is how to handle flow both in the matrix and in the fractures. Using a single-porosity model by discretizing explicitly fractures is a solution, but it generally needs a great number of cells for such a simulation. Cipolla et al. (2009b) and Rubin (2010) propose to use LS-LR-DK (Logarithmically Spaced,

Locally Refined, and Dual Permeability) grid to reduce the number of cells with a single-porosity model simulation. That technique uses large fracture cells (for example, 2 ft in width) to mimic low-aperture fractures (for example, 0.001 ft in aperture). Therefore, equivalent petrophysical properties have to be assigned to these large fracture cells. In this paper, we will analyse the numerical scheme for the fracture discretization, and propose to explicitly discretize the fractures with the same number of cells as in LS-LR-DK grid.

When using a dual-porosity model, a shape factor is required to simulate the matrix-fracture interaction. However, the shape factor, which is based on pseudo-steady-state flow for the matrix-fracture exchange calculation, is not always suitable for shale-gas simulations, because of long transient period due to extremely low matrix permeability. To improve the simulation for matrix-fracture interaction, the multiple interacting continua (MINC) method (Pruess and Narasimham, 1985) is investigated.

It is well known that the MINC method can better handle matrix-fracture exchanges with a dual-porosity model (see, for example, Nanba, 1991; Farhadinia and Delshad, 2010). But recent researches show that the MINC method is not sufficiently accurate for the simulation in shale-gas reservoirs (Cipolla et al. 2009b; Rubin, 2010). In the MINC method (Pruess and Narasimham, 1985), each matrix block is subdivided into several nested "sub-cells", and the connection factors (transmissibilities) between these sub-cells are determined from rectangular based geometry. In this paper, we propose a new technique to improve the MINC accuracy by determining the inter-cell transmissibilities on the basis of the iso-potential (iso-pressure) geometry under pseudo-steady-state regime. This new technique indeed improves the MINC method.

Mathematical model

Let us consider a gas-water two-phase flow problem in fractured media. For simplicity, it is assumed that the gas and water components are present only in their associated phases and adsorbed gas is within the solid phase of rock. In a dual-porosity model, the mole conservation is applied to each component p ($p = g$ for gas and $p = w$ for water) in both matrix and fractured media by the following equations:

$$\frac{\partial}{\partial t}(\phi^m \xi_p^m S_p^m + v_{sg}) + div(\xi_p^m \vec{u}_p^m) + Q_p^{mf} - Q_p^m = 0 \quad (1),$$

$$\frac{\partial}{\partial t}(\phi^f \xi_p^f S_p^f) + div(\xi_p^f \vec{u}_p^f) - Q_p^{mf} - Q_p^f = 0 \quad (2),$$

where the superscript m represents the matrix medium and f represents the fracture medium, ϕ is the effective porosity; S_p is the saturation of the phase p (index p represents also the phase with $p = g$ for gas and $p = w$ for water); ξ_p is the mole density of the phase p; $\vec{u}_p$ is the volumetric velocity vector of the phase p; Q_p is the sink/source term of the component (or phase) p per unit volume of formation; Q_p^{mf} is the exchange term between the matrix and the fracture. v_{sg} corresponds to the gas sorption term, and it appears only in the gas component conservation equation in the matrix media.

For a single-porosity model, Eq.(1) alone is used for the flow simulation in the whole reservoir, with different petrophysical properties in matrix and fracture cells. In a dual-porosity model, if the single-permeability concept is applied, the term $div(\xi_p^m \vec{u}_p^m)^m$ in Eq.(1) is ignored. In the following, we will discuss how to simulate the specific shale gas flow physics with the above model and the numerical discretization aspects that are involved in the implementation of that model.

Incorporation of Gas Adsorption/Desorption

Although gas desorption from kerogenic media has been studied extensively in coalbed methane reservoirs, and several models have been developed for such reservoirs (Clarkson and Bustin, 2010), the sorptive properties of shale are not necessarily analogous to coal (Leahy-Dios et al. 2011). The most commonly used empirical model describing sorption onto organic carbon in shales is analogous to that used in coalbed methane and follows the Langmuir isotherm (Langmuir, 1916).

The sorption term in Eq. (1) is calculated by

$$v_{sg} = (1 - \phi^m - \phi^f)\xi_{sc}\rho_r V_s \quad (3)$$

where V_s is the volume of adsorbed gas in standard conditions per unit mass of solid, ρ_r is the solid rock density, and ξ_{sc} is the gas mole density at standard condition. Considering instantaneous equilibrium sorption with Langmuir isotherm, the dependency of adsorbed gas volume on pressure at a constant temperature is given below

$$V_s = \frac{V_L P_g}{(P_L + P_g)} \tag{4}$$

where V_L is Langmuir volume, P_L is Langmuir pressure, the pressure at which 50% of the gas is desorbed, P_g is the reservoir gas pressure. The Langmuir volume V_L is a function of the organic richness (or TOC).

Incorporation of Geomechnical effect:
Wu et al. (2013) incorporated the impacts of geomechanics on the effective porosity and permeability through mean effective stress, which is defined as the difference between the mean total stress and the formation pressure with a Biot factor. In general, the variation of total stress is much smaller than the variation of pressure during gas production in a shale-gas reservoir. Hence, as a simplified approach, we assume that the variations of effective porosity and permeability are functions of the formation pressure only. The permeability variation behavior due to geomechanics depends on many factors, such as the type of fractures (hydraulic fractures, partially propped fracture, micro fractures) and Young's modulus, etc. (Cipolla et al. 2009a; Winterfeld and Wu, 2013). It is generally recommended using different laws and parameters, based on laboratory experiments, to model the geomechanics effect on the porosity and permeability changes according to the formation, types of fractures, etc.

When a dual-porosity model is used, the micro fractures can be considered either as a part of fractured medium or as a part of matrix medium. The effective geomechanical effect on petrophysical properties should be considered in a cell containing different types of fractures and/or matrix. For practical applications, we incorporate the geomechanics effect using tabulated table to describe the porosity and permeability change as a function of the gas pressure in the simulated cells.

Incorporation of Klinkenberg Effect:
In low-permeability shale gas formations with nano-size pores, gas slippage effect or Klinkenberg effect may change significantly the formation permeability, especially in low reservoir pressure conditions. Klinkenberg effect is incorporated in the gas flow equation by modifying the gas phase permeability as a function of gas pressure (e.g., Wu et al. 1998):

$$k_g = k_\infty \left(1 + \frac{b_K}{P_g}\right) \tag{5}$$

where k_∞ is constant, equal to the absolute gas-phase permeability under very large gas-phase pressure (where the Klinkenberg effect is minimized); and b_K is the Klinkenberg *b*-factor. Although b_K may change with gas nature and pore/threshold size, we adopted a constant b_K factor in the simulation tests below.

Remark: in a tight-matrix, the matrix permeability is subject to both the Klinkenberg effect and the geomechanical effect, with opposite impacts on results. When pressure decreases, the gas permeability increases because of the Klinkenberg effect, but at the same time decreases because of the geomechanical effect. Besides, Klinkenberg effect modifies only the permeability to gas, whereas the geomechanical effect modifies the absolute permeability for both gas and water flows. Precautions should then be taken when incorporating these two effects in a reservoir simulator.

Incorporation of non-Darcy flow:
The gas velocity might be very large inside the fracture, especially in the near-well region, where radial flow increases gas velocity. For high velocity non-Darcy flow, Forchheimer equation is usually used (*e.g.*, Wu, 2002):

$$-\left(\nabla\Phi_g\right) = \frac{\mu_g}{k_{rg}k}\vec{u}_g + \beta_g \rho_g \vec{u}_g \left|\vec{u}_g\right| \tag{6}$$

where β_g is the effective non-Darcy flow coefficient for the gas phase; μ_g is the gas phase viscosity; ρ_g is the gas phase density; k is the absolute permeability; k_{rg} is the gas relative permeability; $\nabla\Phi_g$ is the potential gradient of the gas phase (the potential of a phase p is defined as $\Phi_p = P_p + \rho_p g z$ with P the pressure, ρ the density, g the gravity acceleration, and z the depth), and $\vec{u}_g$ is the gas velocity.

Numerical formulation

The system equations Eqs. (1) and (2) are discretized in space using a control-volume method. Time discretization is carried out using a backward, first-order, fully-implicit, finite-difference scheme. In this section, we will particularly study spatial discretizations for the flow term across an interface between two neighbouring cells (transmissibility calculation) and for the matrix-fracture exchange in a dual-porosity model and with the MINC approach. The analysis for the transmissibility calculation is particularly useful for explicit discretization of fractures with a single-porosity model. The investigation of

MINC method and study new techniques is helpful to improve the calculation of matrix-fracture exchange in a dual-porosity model.

Transmissibility

For simplicity, we consider only the discretization of the transport equation in a single-porosity medium for the study of spatial discretization. By neglecting the sorption term and the matrix-fracture exchange term, the discretization of Eq. (1) on a cell i is given by (the index m is omitted):

$$((\phi\xi_p S_p)_i^{n+1} - (\phi\ \xi_p S_p)_i^n)\frac{V_i}{\Delta t^{n+1}} - \sum_{j\in N_i} F_{p,ij}^{n+1} - Q_{p,i} = 0 \tag{7}$$

where the superscript n denotes the previous timestep, and $n+1$ the current timestep to be solved; Δt^{n+1} is the timestep size; V_i is the volume of the cell i; N_i contains the set of direct neighboring cells (j) of cell i; $F_{p,ij}$ is the flow term between cells i and j; and $Q_{p,i}$ is the sink/source term in cell i.

The flow terms F_{ij} in the above equation are mole fluxes by advective processes. When Darcy's law is applicable, this term is written as (**Fig. 1**):

$$F_{p,ij} = -\int_{\Gamma_{ij}} \lambda_p k \frac{\partial \Phi}{\partial n} d\sigma \tag{8}$$

where Γ_{ij} is the interface between cells i and j, λ_p is the mobility term of phase p, Φ is the potential, and n is the normal direction at the interface Γ_{ij}. Taking a simplified two points flux approximation scheme, the discretization of the flow term is given by:

$$F_{p,ij} = \lambda_{p,i\ j} T_{ij}(\Phi_{p,j} - \Phi_{p,i}) \tag{9}$$

where $\lambda_{p,i\ j}$ is calculated with an upstream scheme; T_{ij} is the transmissibility between cells i and j, calculated with a weighted harmonic average for a two-points scheme (**Fig. 1**):

$$T_{ij} = A_{ij}\frac{k_i k_j}{D_j k_i + D_i k_j} \tag{10}$$

where A_{ij} is the area of the interface between cells i and j; D_i and D_j are respectively the distances from the cell centers i and j to their interface; k_i and k_j are respectively the absolute permeabilities in cells i and j in the direction orthogonal to their common interface.

To simulate discrete fractures, Cipolla et al. (2009b) and Rubin (2010) propose to use LS-LR-DK grid. Larger fracture cells (for example, with a width of 2ft) are used to mimic the actual fractures that are characterized by a very small aperture. Therefore, equivalent fracture permeability and porosity need to be calculated on these fracture cells (and also on matrix cells as their geometric volumes are reduced). For non-Darcy flow, it is also required to recalculate the true gas velocity inside the small fractures.

It is possible to discretize explicitly the fractures without increasing the number of cells and CPU time, by comparison with the LS-LR-DK grid. **Fig. 2** shows two different grids for the fracture discretization. In Grid A, a thicker fracture cell is used for the discretization of the fracture (cells 1, 2 and 3 in red color are the fracture cells). In Grid B the fracture is explicitly discretized with a very thin cell. For Grid A, equivalent porosity is used on the fracture cells so that the porous volume is conserved, and equivalent permeability on the fracture cells is also used so that the fracture conductivity is kept unchanged. For Grid B, such calculations are not necessary. Nevertheless, these two grids have almost the same coefficients in the discretized formula of Eq. (7).

Considering Eq. (7) on cell 1 (a fracture cell), the accumulation terms (the first term in Eq. (7)) are the same for Grid A and Grid B, as ϕV_1 (porous volume) are the same for both grids. The transmissibilities for the flow term around the fracture cell are also (almost) the same. In fact, the transmissibility between fracture cells 1 and 2 (having same length $D_1=D_2$) is given by:

$$T_{12} = \frac{A_{12}k_f}{2D_1} \tag{11}$$

for both grids A and B, since $D_1 = D_2$ and because the fracture permeability k_f in Grid A is changed so that the conductivity (that is, $A_{12}k_f$) is conserved. So we have the same transmissibility along the fracture direction for both grids. The transmissibility perpendicular to the fracture between a fracture cell (Cell 1) and its neighbor (matrix Cell 4) is given by:

$$T_{14} = A_{14}\frac{k_f k_m}{D_4 k_f + D_1 k_m} = \frac{A_{14}k_m}{D_4}\frac{1}{1+\frac{D_1 k_m}{D_4 k_f}} \tag{12}$$

The $\frac{D_1 k_m}{D_4 k_f}$ term can be neglected because the fracture permeability k_f is about 10^7 to 10^8 times higher than matrix permeability k_m, and the distance ratio D_1/D_4 is smaller than 1. So, the transmissibilities towards (perpendicular to) the fracture in both grids are calculated by:

$$T_{14} \approx \frac{A_{14}k_m}{D_4} \tag{13}$$

Therefore, we can consider the transmissibilities around the fracture cells are the same for both grids (Grid A and Grid B), hence no differences are expected between the flow results simulated on these two grids.

In general, it is not recommended to have a big contrast in cell sizes between two neighboring cells to avoid numerical instability. However, it is not the case for fracture cells, because the porous volumes are intentionally kept the same, and the permeability contrast between the fracture and the matrix can largely compensate the contrast between cell sizes. A numerical comparison for different grid systems is given in Example 1 here after.

Matrix-fracture exchange

In a dual-porosity model, the flow exchange term between coupled matrix and fracture cells at a given reservoir location is calculated by:

$$Q_p^{mf} = \lambda_p^{mf}\sigma(\Phi_p^m - \Phi_p^f) \tag{14}$$

where λ_p^{mf} is the mobility term to phase p; Φ_p^m and Φ_p^f are the matrix and fracture potential respectively; σ is the shape factor, characterized by the geometry of matrix block(s) and the matrix permeability under pseudo-steady-state flow. However, as the matrix permeability in the shale gas reservoir is very low, the flow can be in transient regime during several years before stabilizing in a pseudo-steady-state regime. The dual-porosity model is generally not accurate enough for flow simulations in the shale gas reservoir using a shape factor obtained under pseudo-steady-state condition. One possible improvement is using the MINC method.

Pruess and Narasimham (1985) introduced the concept of Multiple INteracting Continua (MINC) to model heat and multiphase fluid flow in fractured porous media. The MINC concept is able to describe gradients of pressures, temperatures, or concentrations near matrix surface and inside the matrix by further subdividing individual matrix blocks into one- or multidimensional strings of nested meshes, as shown in **Fig. 3**. Therefore, the MINC method treats interporosity flow in a fully transient manner by computing the gradients which drive interporosity flow at the matrix-fracture interface. As a result, the MINC model in general provides a better numerical approximation for transient fracture-matrix interactions than the double-porosity model. This method was applied to various studies of fractured reservoirs (see, for example, Nanba, 1991; Farhadinia and Delshad, 2010). But recent works show that this method is not very accurate for extremely-low-permeability shale-gas reservoirs (Cipolla et al. 2009b; Rubin, 2010).

In the MINC approach, a matrix block is subdivided, according to a criterium based on the distance from the fracture, in order to build a pattern of nested meshes (**Fig. 4**). The flow transport is governed by Eq. (1) in the matrix media, and its discretization is under the form Eq. (7). The key point of the MINC method is the approximation of the flow term F_{ij} between two neighboring nested meshes expressed by Eq. (8). Considering a square matrix block (2D problem) and assuming the matrix permeability k_m is constant, the discretization form of the flow F_{ij} between two neighboring sub-cells i and j is still given by Eq. (9) with the transmissibility T_{ij} given by:

$$T_{ij} = k_m\frac{A_{ij}}{D_{ij}} \tag{15}$$

where A_{ij} is the area of the interface between these two sub-cells, and D_{ij} is the "average" distance between the two sub-cells for the normal potential derivative $\frac{\partial\Phi}{\partial n}$ calculation. This approach is reasonably accurate, if the potential is constant in each ring (dashed lines in **Fig. 4**). It is generally true for sub-cells near the boundary, especially in early-time. But near the center, the iso-potential cannot be described by a square (or a rectangle), and it is more close to a circle (or an ellipse for a rectangular matrix block). **Fig. 5** shows the iso-potential lines calculated on a quarter of a square block with a constant pressure on the boundary, after 10% and 50% of recoverable gas have been produced from the matrix block.

To improve the MINC method, we propose to subdivide a matrix block on the basis of iso-potential. This concept is helpful for the simulation in ultra-low permeability reservoirs like shale-gas reservoirs. **Fig. 6** presents the schematic of the new technique. We use iso-potential lines at the early-time production near the boundary, and late-time near the center with a progressive change from the boundary to the center.

For a square matrix block, we can approximately generate iso-potential lines with a quasi-steady-state flow by putting a sink/source at the center. **Fig. 7** shows the iso-potential lines of a quasi-steady-state simulation. These lines are very similar to those obtained at 50% of gas production by a diffusion process (**Fig. 5b**). The advantage of using a quasi-steady-state flow simulation is that we can determine the transmissibility without using geometrical computation. Let P_i^s and P_j^s be respectively the average pressure of sub-cells *i* and *j* located on two distinct iso-potential lines, and Q_{ij}^s be the flow rate under the quasi-steady-state regime between these two inner sub-cells, then the flow transmissibility between these two sub-cells is determined by identification with the Darcy's law:

$$T_{ij} = \frac{Q_{ij}^s}{(P_j^s - P_i^s)} \tag{16}.$$

Eq. (16) is not applied to the outermost sub-cells, where iso-potential lines at early-time are close to rectangles. Eq. (15) is still applied to outermost sub-cells. For the innermost sub-cell, the connection with its neighboring sub-cell is very similar to the shape factor widely used in the dual-porosity model. The shape factor has been greatly discussed in the literature (see, for example, Wuthicharn and Zimmerman, 2011), and many choices are possible. For example, we can choose a pressure so that its iso-value line separates the innermost sub-cell in two equal volumes. This choice is roughly equivalent to use a pressure at a distance of $\mathbf{0.5\sqrt{2}}R$ from the center, where R is the equivalent radius of the innermost volume. This approach can improve considerably the standard MINC method for simulations in ultra-low permeability reservoirs.

In practice, a pseudo-steady-state potential distribution in a matrix block with a constant potential outer boundary condition can be obtained by a numerical fine grid simulation, if analytical solution is not available. Then, we define the sub-cells according to the volumes delimited by the distribution of iso-potential lines between the matrix block center and boundary. In applications, it is not necessary to know the form of a sub-cell. The average pressure in a sub-cell can be easily determined, using all sub-cell pressures delimited by the iso-potential values which separate sub-cells. The flow Q_{ij} between sub-cells can be considered constant for a quasi-steady-state flow, and is equal to the sink/source rate.

Numerical results

In the first example, we study the effect of grid systems with a single-porosity model for the simulation of hydraulic fractures. Then we simulate gas production in a multi-stage fractured horizontal well with the presence of induced secondary fractures and/or natural micro-fractures in a stimulated reservoir volume (SRV), and study relevant physical processes and investigate the MINC approach for shale gas reservoir simulation. If micro-fractures are present, they are considered as a part of the matrix medium and they increase the effective matrix permeability and porosity.

Example 1.

Considering a half-panel between two fractures in a multi-fractured system as shown in **Fig. 8**. The size of the considered zone is 250 ft in x-direction, 1000 ft in y-direction and 50 ft in z-direction. A fully penetrated fracture with half length of 250 ft and width of 0.01 ft is located on the left side of magnified half-panel shown in **Fig. 8**. The horizontal well is located in the middle layer. The fracture permeability is 50 D, and the matrix permeability is 0.0001 mD. It is assumed that the flow from the tight matrix to the horizontal well is neglected, and only fracture contributes to the gas production. The reservoir is saturated with gas and water, but water is at an irreducible saturation value and considered as an immobile phase. The initial reservoir pressure is 3800 psi, and the bottom-hole well pressure is 1000 psi.

In this example, we will study gridding techniques for simulating gas flow with a single-porosity model. Although a fractured reservoir can be correctly simulated using a single-porosity model with very small fracture cells, limitations may be encountered for field cases involving a large number of cells. Cipolla et al. (2009b) and Rubin (2010) use LS-LR-DK grid and get quite satisfactory results. Here, we use an alternative grid by discretizing explicitly the hydraulic fractures.

A fine grid system, with small matrix cells close to the fracture, starting with a 0.02-foot cell thickness, and also small cells near the fracture extremities, is used for computing reference solutions. The vertical direction is also discretized with 15 cells.

First, we simulate this half-panel with a "coarse" grid with 7 cells in x-direction, 13 cells in y-direction and 5 cells in z-direction (**Table 1**). For the "coarse" model, two kinds of grid are considered with slightly different sizes of the fracture cells and their neighbors. In the grid named "Coarse 1", fracture cell width is 1ft, and equivalent permeability and porosity are

assigned to these fracture cells. The width of the neighboring matrix cell is 1.2ft. In the grid named "Coarse 2", the fracture is explicitly discretized with very small cells, having a width of 0.005 ft (*i.e.* half the estimated value of the actual fracture aperture), and the width of the neighboring matrix cells is 2.195ft. **Fig. 9** presents the simulation results. Globally, both coarse grid simulation results are considered satisfactory. A zoom in early time shows that results are slightly better with "Coarse 2" grid than with "Coarse 1" grid (the difference is insignificant), and in late-time, small differences are found between the reference fine grid simulation and the coarse grid simulations. **Fig. 10** presents the cumulative gas production. A different around 4% is observed between the reference fine grid simulation and the coarse grid simulations. This difference may be related to the continuous flow support from the matrix media far from the fracture. In the case of a fracture network, which will be shown below, the difference is negligible. Nevertheless, the two coarse grid simulations give very close results. The advantage of realistic "Coarse 2" grid is that it is not necessary to calculate equivalent properties in the fracture cells, which makes the model building easier. In addition, the assignment of actual properties to the fracture cells of that grid gives the possibility to directly simulate complex physics such as non-Darcy flow. The CPU times for both coarse grid simulations are the same (CPU time is 0.686 s for "Coarse 1" grid and 0.689 s for "Coarse 2" grid). The small fracture cells of "Coarse 2" grid do not increase the stability and convergence issues.

As only gas phase is mobile, the problem is considered as a single-phase one. So, we investigate the possibility of simulation using a 2D grid with 105 cells (**Table 1**). In this example, the difference between 2D and 3D simulations is the handling of the flow connections between the horizontal well and the intersected fractures, which are linear with a 2D grid and radial with a 3D grid. However, as the fracture conductivity is almost infinite (the fracture permeability is 10^8 times higher than the matrix permeability), the accurate modeling of the intersection between the well and the fracture does not seem to be very important, because all gas inside the fracture is quickly produced by the well. The simulation result of the 2D "Coarse" grid is also shown in **Fig. 9**. Due to the high fracture conductivity, very satisfactory results with the 2D grid are obtained. **Fig. 8** also presents the pressure distribution at 3000 days. Coarse and fine grid simulations give quite similar results.

Now we compare different grid simulations in a domain with a fracture network. The fracture spacing is 200 ft (**Fig. 11**), and a pseudo-steady-state flow regime is reached much earlier than in the case with a single hydraulic fracture. **Figs. 12** and **13** compare the gas flow rate and cumulative gas production simulated on a grid of type 2D "Coarse" and on a very fine grid. This time, the two models give very close results, even at late times for the cumulative gas production.

The above simulations show that using a 2D "coarse" grid with an explicit discretization of the fractures can give globally satisfactory results, especially for the simulation with a fracture network. In the following examples, simulation with a fracture network is studied. The explicit 2D grid (*i.e.* 2D "Coarse 2" grid type) is used to study shale-gas-flow physical phenomena, and to investigate dual-porosity and MINC approaches.

Example 2.

We now consider a shale-gas reservoir with an effective permeability (including matrix and micro-fractures) of 0.0001 mD. Three cases of a multi-stage fractured horizontal well are considered with a same stimulation volume of 1400 ft by 1000 ft (the reservoir height is 300 ft). The permeability in the hydraulic fracture is 50 D and the permeability in the secondary fracture is 2 D.

In Case 1, 14 hydraulic fractures with a spacing of 100 ft are created, and 10 secondary fractures perpendicular to the hydraulic fracture are induced with also a spacing of 100 ft (**Fig. 14a**). In Case 2, 7 hydraulic fractures are created with a spacing of 200 ft, and 5 secondary perpendicular fractures with also a spacing of 200 ft are induced (**Fig. 14b**). In Case 3, 4 hydraulic fractures and 3 secondary fractures with a spacing of 350 ft are created. Outside the stimulated volume, no fractures are considered (except micro-fractures, which are included as a part of the matrix medium). In all cases, the hydraulic fracture half-length is 500 ft (total length of 1000 ft), and the total length of a secondary fracture is 1400 ft (**Fig. 14**).

The initial reservoir pressure is 3800 psi. The bottom-hole well flowing pressure (BHP) is fixed to 1000 psi.

Simulation with a Single-Porosity Model

The simulation was first performed with a single-porosity model using a local grid refinement around the fracture with a grid of type "Coarse 2D" in described Example 1. **Fig. 15** shows the gas production in these three configurations. It is clear that higher productions are observed when more hydraulic fractures are created. Increasing the number of hydraulic fractures enhances gas production.

Simulation with a Dual-Porosity Model

Now, we study the simulation with a dual-porosity model that uses the grid shown in **Fig. 16** for these 3 cases. In this model, the shape factor σ for calculating matrix-fracture interaction is given by:

$$\sigma = \frac{\mathbf{10}}{a^{\mathbf{2}}} + \frac{\mathbf{10}}{b^{\mathbf{2}}} \quad (17),$$

where a and b are the 2D matrix block dimensions. The simulation results are presented in **Fig. 17**. Comparing with the reference solutions obtained with a single-porosity model, we find that the errors are very large, especially for the large fracture spacing case. These errors are mainly related to the inaccurate simulation of matrix-fracture exchanges with a dual-porosity model, due to the extremely-low reservoir permeability, that induces an unsteady-state flow regime during a very long time.

In a conventional permeable reservoir, the values of the shape factor have no great impact on production forecasts because the transient states of the matrix-fracture exchange processcan be neglected for a single-phase depletion process. However, such transient phenomena cannot be neglected in an unconventional (very-low-permeability) shale-gas reservoir. **Fig. 18** shows the simulation for Case 2 with a shape factor that is reduced by a factor of 0.4 and 0.8, taking into account the fact that cumulative production is highly overestimated with the initial shape factor. Although the "average" behavior can be improved, the difference is still very large during the 14 years production. It is not possible to obtain reasonable results using a dual-porosity model with a constant shape factor. Correct simulation of matrix-fracture interaction is the key point for the unconventional reservoir simulation with a dual porosity model. Example 3 hereafter will study the MINC approach and its improvement for an accurate simulation of matrix-fracture exchanges.

Simulation of Desorption

We consider a high TOC reservoir with the sorption curve shown in **Fig. 19**. **Fig. 20** compares the desorption effects with a BHP of 1000 psi or of 500 psi for the 3 cases. The incremental gas production depends strongly on the fracture spacing. When the fracture network is dense, the pressure drops faster and more gas is desorbed, contributing to the additional gas production. In Case 1, the incremental production due to gas desorption is 17% for BHP = 1000 psi and 22% for BHP = 500 psi. In Case 2, the incremental production is reduced to 11% and 13% for BHP = 1000 psi and 500 psi respectively. In Case 3, the incremental production is only 7% and 8% for BHP=1000 psi and BHP=500 psi. A small fracture spacing (or a large number of hydraulic fractures) does not only increase gas production due to reservoir depletion, but also produces more additional gas due to desorption at low reservoir pressures. In this example, the contribution from gas desorption is in the same order as the contribution of an additional pressure drop of 500 psi.

Matrix permeability

Figure 21 presents the cumulative gas production with a matrix permeability of 0.001 mD, 0.0001 mD and 0.00001 mD for the same three cases. The impact of matrix permeability is significant. A higher matrix permeability, either linked to a higher reservoir quality or to the presence of micro-fractures, improves greatly the gas recovery. Hence, it is important to create and/or reactivate micro-fractures to enhance shale gas production. The matrix permeability is also directly related to the geomechanical effect presented below.

Simulation of Geomechanical Effects

The geomechanical effect resulting from pressure depletion diminishes the permeability of the naturally-microfractured matrix. The impact can be 1 to 2 orders of magnitude (Wang et al. 2009). **Fig. 22** shows three curves of permeability variation k_m/k_{init} in the matrix medium (including micro-fractures), as a function of reservoir pressure, where k_{init} represents the initial reservoir permeability and k_m is the current permeability. Curve M2 characterizes a more stress-sensitive formation case than curve M1, and curve M3 represents the most stress-sensitive case.

Figure 23 presents the simulation results. The geomechanical effect is significant, according to the sensitivity to stress (or the reservoir pressure) of the (possibly) micro-fractured matrix permeability. The production is more reduced with a small number of hydraulic fractures (large fracture spacing). For the most stress-sensitive case (curve M3), the total production is reduced by 36% for Case 1 (fracture spacing of 100 ft), by 47% for Case 2 (fracture spacing of 200 ft), and by more than a half (51.4%) for Case 3 (fracture spacing of 350 ft). Actually, the production rate per fracture with a small number of fractures is higher than the production per fracture with a large number of fractures. So, the pressure in the matrix drops lower in the case of a small number of fractures. This higher pressure drop results in a higher (geomechanical) decrease of the matrix permeability close to the hydraulic fractures, with a direct impact on gas production.

Example 3.

In this example, we consider a uniform fracture network in a large stimulated reservoir domain of 3000 ft by 2000 ft as shown in **Fig. 24**. The reservoir thickness is 300 ft. The fracture spacing is assumed to be 200 ft for both hydraulic and secondary fractures. This domain holds 15 hydraulic fractures (perpendicular to the horizontal well) and 10 induced secondary fractures.

This case is considered to study the MINC approach for shale gas reservoir simulation. In order to study the accuracy of the MINC method, we use again a very fine grid simulation as the reference solution. The permeability is always 50 D for the

hydraulic fractures, 2 D for secondary fractures and different matrix permeabilities are considered. Some relevant physical phenomena related to low permeability porous media (Klinkenberg effect), to fractured reservoirs (non-Darcy flow) are also investigated in this example.

Simulation with MINC Method

In the previous example, it is shown that a dual-porosity model cannot simulate correctly the matrix-fracture interaction due to the extremely-low matrix permeability. In the MINC approach, the matrix block is subdivided into small sub-volumes from the matrix-fracture boundary to the block centre.

Figure 25 presents the simulation results with the MINC method (Pruess and Narasimhan, 1985) with different matrix subdivisions. The dual-porosity model is not accurate. MINC4 model, which divides the matrix block into 4 sub-volumes, gives much better results. The progress is significant. The prediction of MINC8 model, which divides the matrix block into 8 sub-volumes, are slightly closer to the reference solution than MINC4 model prediction. If we continue the subdivision of the matrix block, we find that the MINC approach can no further improve the results significantly. The simulation with MINC30 model, which divides the matrix block into 30 sub-volumes, shows very little difference if compared with the prediction of MINC8 model. The error seems small, but still represents around 6% at 500 days and 15% at late times for the MINC30 model. This error has also an impact on cumulative production, especially for the 1000-2000 days period (**Fig. 26**).

Although the MINC approach gives much better results than the dual-porosity model, the remaining problem is that the MINC method does not converge to the true solution with a refinement of block subdivision. This is because MINC subdivides the matrix block only in one direction orthogonal to matrix block boundary, and lateral flow interactions are not taken into account. If the average pressure value is erroneous due to potential or flow variations within a given ring, this error remains whatever the refinement of matrix block volume subdivision. The error with MINC method is emphasized in shale-gas reservoir simulations because of the long transient effect in extremely low permeability reservoirs.

Figures 27 and **28** show the results obtained with the improved MINC technique implemented with 4 matrix block subdivisions. The curve "MINC4_Iso_P" represents that simulation with a subdivision based on iso-potential and transmissibilities determined from a (pseudo)-steady-state flow. "MINC4_Iso_P" model is significantly more predictive than the standard MINC approach with 4 subdivisions (curve "MINC4"), and it is even much better than the standard MINC method using 30 subdivisions (curve "MINC30"). **Figs. 29** and **30** show the improved technique with 8 subdivisions. Excellent results are obtained for both gas flow rates and cumulative gas productions. The error on production rate is only 0.4% at 500 days and 0.5% in late time production.

Klinkenberg Effect

Figure 31 shows the permeability variation as a function of pressure due to the Klinkenberg effect, where the Klinkenberg b_K-factor is fixed at 10^6 psi^{-1}. Permeability variation is increased for low-permeability formations where pressure must drop severely to satisfy a given production rate. However, in reservoir conditions, the reservoir permeability varies only 10% from 0.0001 mD to 0.00011 mD when pressure drops from 3800 psi to 1000 psi.

Figure 32 shows the Klinkenberg effect on cumulative production with different initial reservoir permeabilities. When the permeability is high, the Klinkenberg effect can be neglected. The impact of Klinkenberg effect becomes significant only in very low permeability reservoir (for example, Km = 0.00001 mD). In ultra-low-permeability reservoirs, gas flow is concentrated in the near-fracture zone and induces a high pressure drawdown. So, the gas permeability is increased in this area due to Klinkenberg effect, which helps the gas transfer from the inner zones of matrix blocks to the fractures. Even though the Klinkenberg effect is observed in ultra-low-permeability reservoirs, the resulting incremental gas production is fairly low, *i.e.* only 8% in 12 years, and this increment is mainly produced during the late-time period. The Klinkenberg effect may be important if the bottom-hole well pressure can be drawn down to very low values.

Klinkenberg and geomechanical effects on production are opposite . When reservoir pressure drops, the Klinkenberg effect increases the gas permeability in the tight matrix medium whereas the geomechanical effect decreases the permeability of the matrix blocks including natural micro-fractures. It may be difficult to distinguish these two effects from laboratory studies. Globally, the permeability of matrix blocks (including the tight matrix and natural micro-fractures) decreases when the pressure gets lower. That is, the Klinkenberg effect could be neglected in preliminary evaluations of shale gas production.

Non-Darcy Flow

The contribution of the inertia term depends on the non-Darcy flow coefficient β_g in Eq.(6). We use the correlation proposed by Evans and Civan (1994) which is given by:

$$\beta_g = \frac{1.485\times10^9}{k_f^{1.021}} \quad (18)$$

where the unit of the fracture permeability is (mD) and the unit of β_g is (ft^{-1}). **Fig. 33** presents the effects of non-Darcy flow for a fracture permeability of 2D, 20D and 200D. For a fracture permeability k_f = 200 D, β_g is 5746 ft^{-1}; for k_f = 20 D, β_g is 60307 ft^{-1}; and for k_f = 2 D, β_g is 632958 ft^{-1}. When fracture permeability is high, gas flow is fast in the fracture, but the non-Darcy flow coefficient is low. So the impact of non-Darcy flow is negligible and is not observed in these cases.

Non-Darcy flow effect is maximized for high gas flow velocities in fairly-low-permeability fractures. We simulate that situation by considering the case of a matrix permeability k_m equal to 0.01 mD, in order to supply more gas to the fracture. **Fig. 34** shows the simulation results for k_f = 2 D, 20 D and 200 D respectively. A small difference is found for k_f = 20 D and 200 D, due to the high gas velocity inside the fracture. However, a matrix permeability as high as 0.01 mD does not seem representative for a shale-gas reservoir. Hence, we may conclude that the impact of non-Darcy flow in shale-gas reservoirs is globally not significant.

In this paper, gas flow from the fracture to the horizontal well is not considered. However, the gas velocity is maximized in the near-well region due to radial flow towards the well. Hence, although it has not been evaluated in this paper, the effect of non-Darcy flow in the well vicinity might be significant.

Summary and Conclusions

This paper discusses a mathematical model for the simulation of gas production from low-permeability fractured unconventional shale-gas reservoirs. This model incorporates several relevant physical processes, such as adsorption/desorption, geomechanics effect, Klinkenberg effect and non-Darcy flow. Numerical simulation techniques are also addressed.

It is possible to efficiently simulate gas production from hydraulic fractures with thin fracture cells and relatively large neighboring matrix cells. The contrast in size between a fracture cell and its neighbors is compensated by the contrast between the fracture and matrix permeabilities, and has no impact on the numerical stability issue.

The standard dual-porosity model, where the shape factors are determined with a pseudo-steady-state regime, is not suitable to properly model very low permeability fractured reservoir. The MINC method can improve significantly the capability of a dual-porosity model to predict matrix-fracture flow exchanges. But it is still not sufficiently accurate for the flow simulation in extremely-low permeability reservoirs. A refined subdivision of the matrix blocks cannot improve the MINC method.

A new technique is proposed to improve the accuracy of the MINC method for application to shale-gas reservoirs. The subdivision of a matrix block is based on iso-potential (or iso-pressure) of a steady-state or a pseudo-steady-state flow. This new technique improves significantly the standard MINC approach for the simulation of shale-gas production.

Gas desorption from organic matter has an impact on the ultimate gas recovery. Reducing the fracture spacing (or increasing the number of hydraulic fractures) can accelerate the desorption process.

Depending on formation and its stress sensitivity, the gas production can be dramatically reduced due to geomechanical effect. The geomechanics effect on micro-fractures and the tight matrix (and possibly-unpropped hydraulic fractures) has a significant impact on gas production. Beside that effect, reactivation of natural fractures is however helpful to increase the gas production.

Klinkenberg effect has generally a small impact on gas production, except for very low reservoir permeability and low bottom-hole well pressure.

Non-Darcy flow does not either have a significant impact in shale-gas reservoirs. However, that conclusion does not concern the immediate near-wellbore region, which has not been considered in this study.

Nomenclature

A_{ij} = *interface areas between two gridblocks (cells) i and j*
a = *matrix block dimension*
b = *matrix block dimension*

b_K = *Klinkenberg factor*
D = *distance from a cell center to its interface with a neighboring cell*
$F_{p,ij}$ = *flow component of fluid p across an interface between gridblocks (or cells) i and j*
g = *gravity*
k = *absolute permeability*
k_g = *gas phase absolute permeability*
k_{init} = *initial reservoir permeability*
k_{rp} = *relative permeability to phase p*
k_∞ = *absolute gas permeability at large gas pressure*
P = *pressure*
P_L = *Langmuir pressure*
P^s = *pressure in a steady-state or pseudo steady-state regime*
Q = *source/sink term*
Q_p^{mf} = *matrix-fracture interaction for phase p*
Q^s = *flow in a steady-state or pseudo steady-state regime*
S = *fluid saturation*
t = *time*
Δt = *time step*
V_i = *volume of gridblock (cell) i*
V_L = *Langmuir volume*
V_s = *volume of adsorbed gas in standard condition par unit mass of solid*
$\vec{u}_p$ = *Darcy's volumetric velocity of phase p*
v_{sg} = *gas sorption term (mole)*
z = *depth (vertical direction)*

β_g = *effective non-Darcy flow coefficient for the gas phase*
ϕ = *effective porosity of formation*
Φ = *flow potential*
T_{ij} = *transmissivity between gridblocks (cells) i and j*
$\lambda_{p,ij}$ = *mobility of phase p between gridblcoks i and j*
μ = *viscosity*
σ = *shape factor*
Γ_{ij} = *interface between two gridblocks (cells) i and j*
ξ = *mole density*
ξ_{sc} = *gas mole density at standard condition*
ρ_r = *solid rock density*

subscript
f = *denote fracture*
g = *gas*
i = *gridblock (cell) i*
j = *gridblock (cell) j*
m = *denotes matrix*
n = *time level*
p = *index of fluid phase*
w = *water*

Acknowledgement
This work was supported in part by IFP Energies Nouvelles and by EMG Research Center of Petroleum Engineering Department at Colorado School of Mines.

References:
Andrade, J., Civan,F., Devagowda, D. and Sigal,R. (2010) "Accurate Simulation of Shale-Gas Reservoirs" SPE 135564 presented at the SPE ATC&E, Florence, Italy, Sept. 19-22.

Blasingame, T.A. (2008) “The Characteristic Flow Behavior of Low-Permeability Reservoir Systems,” SPE 114168, presented at the 2008 SPE Unconventional Reservoirs Conference held in Keystone, Colorado, U.S.A., 10–12 February.

Bustin, R.M., Bustin, A.M.M., Cui, X., Rose, D.J.K. and Murthy Pathi, V.S. (2008) “Impact of Shale Properties on Pore Structure and Storage Characteristics”, SPE 119892 presented at the SPE Gas Production Conf., Nov. 16-18, Fort Worth, TX.

Clarkson, C.R. and Bustin, R.M. (2010) “Coalbed Methane: Current Evaluation Methods, Future Technical Chanllenges” SPE 131791 presented at the SPE Unconventional Gas Conf., Pittsburgh, Pennsylvania, USA, Feb. 23-25.

Cipolla, C.L., Warpinski, N.R., Mayerhofer, M.J., Lolon, E.P. and Vincent, M.C. (2009a) “The Relationship Between Fracture Complexity, Reservoir Properties, and Fracture Treatment Design”, SPE 115769 presented at the SPE ATC&E, Denver, Colorado, U.S.A.

Cipolla, C.L., Lolon, E.P., Erdle, J.C. and Tathed, V. (2009b) "Modeling Well Performance in Shale-Gas Reservoirs", paper SPE 125532 presented at the SPE/EAGE Reservoir Characterization and Simulation Conf. Abu Dhabi, UAE, 19-21 Oct.

Cipolla, C.L., Lolon, E.P., Erdle, J.C. and Rubin, B. (2010) "Reservoir Modeling in Shale-Gas Reservoirs", SPE Reservoir Evaluation & Engineering, August. pp638-653.

Darishchev, A., Lemouzy, P., and Rouvroy, P. (2013): “On Simulation of Flow in Tight and Shale Gas Reservoirs” SPE 163990 presented at the SPE Middle East Unconventional Gas Conference and Exhibition held in Muscat, Oman, 28–30 January.

Evans, R.D. and Civan, F. (1994) “Characterization of Non-Darcy Multiphase Flow in Petroleum Bearing Formation”, Final Report, work performed under contract No. DE-AC22-90BC14659, prepared for U.S. Department of Energy Assistant Secretary for Fossil Energy, April.

Farhadinia, M.A. and Delshad, M. (2010) “Modeling and Assessment of Wettability Alteration Processes in Fractured Carbonates Using Dual Porosity and Discrete Fracture Approaches” SPE 129749 presented at the SPE Improved Oil Reco., Tulsa, OK, USA, 24-28 April.

King, E.G. (2010) “Thirty Years of Gas Shale Fracturing: What Have We learned?” SPE 133456, presented at the SPE Annual Technical Conference and Exhibition, Florence, Italy, 19-22 September.

Klinkenberg, L.J., “The Permeability of Porous Media to Liquids and Gases,” in API Drilling andProduction Practice, 200–213, 1941.

Langmuir, I., “The constitution and fundamental properties of solids and liquids”, *Journal of the American Chemical Society*, 38 (11): 2221–2295, 1916.

Leahy-Dios, A., Das, M., Agarwal, A. and Kaminsky, R. D. (2011) “Modeling of Transport Phenomena and Multicomponent Sorption for Shale Gas and Coalbed Methane in an unstructured Grid Simulator,” SPE 147352, presented at the SPE Annual Technical Conference, Denver, Colorado, 30 Octomber-2 November.

Mengal, S.A. and Wattenbarger, R.A. (2011) “Accounting For Adsorbed Gas in Shale Gas Reservoirs”, SPE 141085, presented at the SPE Middle East Oil and Gas Show and Conference held in Manama, Bahrain, 25–28 September.

Mirzaei, M. and Cipolla, C.L. (2012) “A Workflow for Modeling and Simulation of Hydraulic Fractures in Unconventional Gas Reservoirs”, SPE 153022 presented at the SPE Middle East Unconventional Gas Conf. and Exhi., Abu Dhabi, UAE, Janv. 23-25.

Moridis, G.L., Blasingame, T.A. and Freeman, C.M. (2010) “Analysis of Mechanisms of Flow in Fractured Tight-Gas and Shale-Gas Reservoirs”, paper SPE 139250 presented at the SPE Latin American & Caribbean Petroleum Eng. Conf., Lima, Peru, 1-3 Dec.

Nanba, T. (1991) “Numerical Simulation of Pressure Transient in Naturally Fractured Reservoirs with Unsteady-State Matrix-to-Fracture Flow”, SPE 22719 presented at the 66th ATC&E, Dallas, USA, Oct. 6-9.

Passey, Q.R., Bohacs, K.M., Esch, W.L., Klimentidis, R. and Sinha, S. (2010) “From Oil-Prone Source Rock to Gas-Producing Shale Reservoir – Geological and Petrophysical Characterization of Unconventional Shale-Gas Reservoirs”, SPE 131350 presented at the CPS/SPE Internation Oil and Gas Conf. and Exhi., Beijing, China, June 8-10.

Pruess, K. and Narasimhan, T.N. (1985) “A Practical Method for Modeling Fluid And Heat Flow in Fractured Porous Media,” *Soc. Pet. Eng. J.,* 25, 14-26.

PumaFlow (2012) “PumaFlow Reservoir Simulator Reference Manual”, Beicip-Franlab.

Rubin, B. (2010) “Accurate Simulation of Non-Darcy Flow in Stimulated Fractured Shale Reservoirs,” SPE 132093, presented at the SPE Western Regional Meeting held in Anaheim, California, USA, 27–29 May.

Soeder, D.J. (1988) “Porosity and Permeability of Eastern Devonian Gas Shale,” *SPE Formation Evaluation*, pp. 116-124, March.

Wang, F.P., Reed, R.M., Jackson, J.A. and Jackson, K.G. (2009) “Pore Networks and Fluid Flow in Gas Shales,” SPE 124253, presented at the 2009 SPE Annual Technical Conference and Exhibition held in New Orleans, Louisiana, USA, 4–7 October.

Winterfeld, P.H. and Wu, Y.S. (2013) “Simulation of CO2 sequestration in brine aquifers with geomechanical coupling” Book Chapter in “Computational Models for CO2 Sequestration and Compressed Air Energy Storage,” Taylor & Francis /CRC press within the Sustainable Energy Developments series, edited by Bundschuh and Rafid Al-Khoury, in press.

Wu, Y.S., Pruess, K. and Persoff, P. (1998) "Gas Flow in Porous Media with Klinkenberg Effects", Transport in Porous Media, vol. 32. pp117-137.

Wu, Y.S. (2002) “Numerical Simulation of Single-Phase and Multiphase Non-Darcy Flow in Porous and Fractured Reservoirs,” *Transport in Porous Media*, Vol. 49, No. 2, 209-240.

Wu, Y.S. and Fakcharoenphol, P (2011) "A Unified Mathematical Model for Unconventional Reservoir Simulation", SPE 142884, presented at the SPE EUROPEC/EAGE Annual Conf. & Exhi., Vienna, Austria, May 23-26.

Wu, Y.S., Wang, C., Li, J. and Fackahroenphol, P. (2012) “Transient Gas Flow in Unconventional Gas Reservoirs,” SPE-154448, presented at the EAGE Annual Conference & Exhibition incorporating SPE Europec held in Copenhagen, Denmark, 4–7 June.

Wu, Y.S., Li, J., Ding, D.Y., Wang, C. and Di, Y. (2013) “A Generalized Framework Model for Simulation of Gas Production in Unconventional Gas Reservoirs”, SPE 163609, presented at the SPE Reservoir Simulation Symposium, The Woodlands, TX, 18-20 Feb.

Wuthicharn, K. and Zimmerman, R.W. (2011) “Shape Factors for Irregularly Shaped Matrix Blocks”, SPE 148060 presented at the SPE Reservoir Characterization and Simulation Conf. and Exhi., Abu Dhabi, UAE, 9-11 Oct.

Table 1 – “Coarse” grid system around the fracture for the simulations in Example 1*

	Dx (ft)	Dy (ft)	Dz (ft)
Coarse 1	**1** 1.2 4 10 25 60.8 148	250 250 150 100 **100 100 50 50 100 100** 100 150 250 250	**50 50 50 50 50**
Coarse 2	**0.01** 2.19 4 10 25 60.8 148	250 250 150 100 **100 100 50 50 100 100** 100 150 250 250	**50 50 50 50 50**
Coarse 2D	**0.01** 2.19 4 10 25 60.8 148	250 250 150 100 **100 100 50 50 100 100** 100 150 250 250	**250**

* Bold numbers correspond to the discretization of the fracture

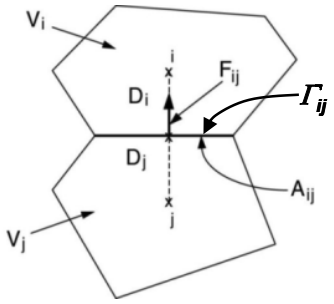

Figure 1—Transmissibility calculation using a two-points flux approximation scheme

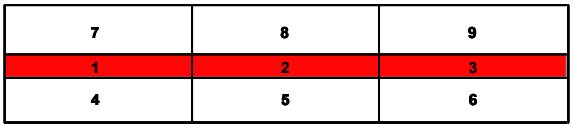

a). Grid 1 – the fracture is discretized with a relatively larger cells (red cells).

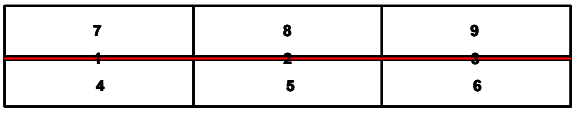

b). Grid 2 – the fracture is explicitly discretized with very thin cells (red cells).

Figure 2—Discretization of the fracture

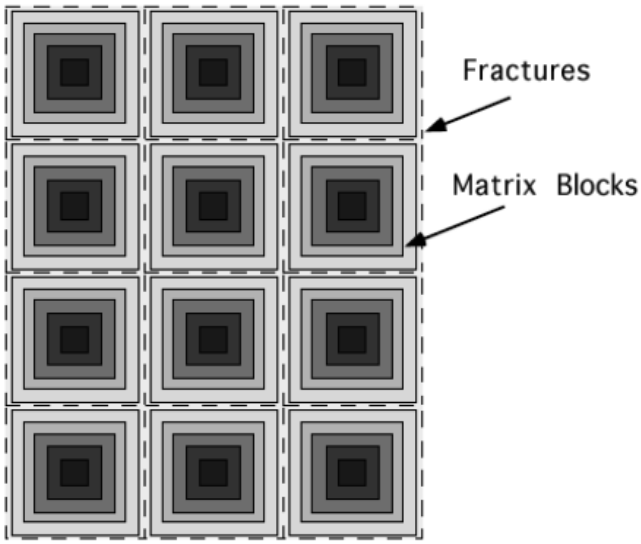

Figure 3--Schematic of MINC concept (Pruess and Narasimham, 1985)

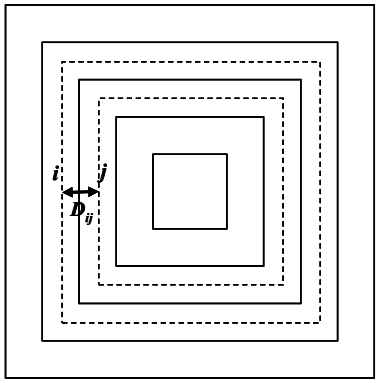

Figure 4—Calculation of the connection factor (transmissibility) in MINC

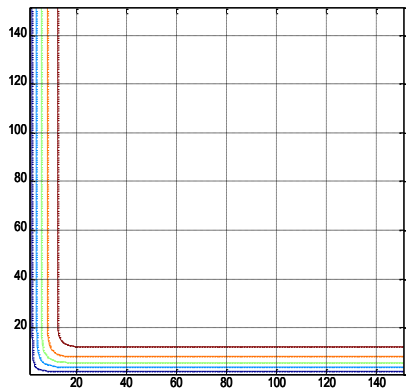

5a). Iso-potential lines at 10% of gas production from the matrix block

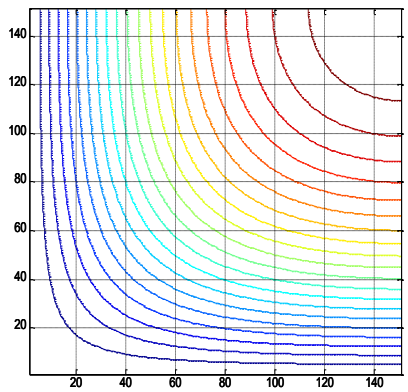

5b). Iso-potential lines at 50% of gas production from the matrix block

Figure 5—Iso-potential lines in a quarter of a square matrix block

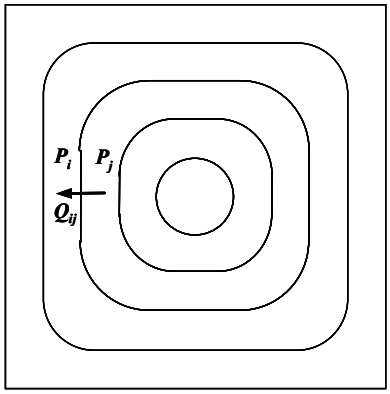

Figure 6—Schematic of the new technique to improve the MINC approach

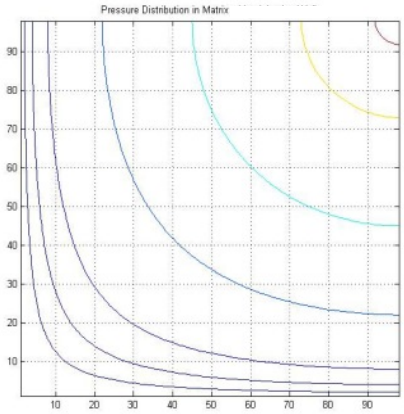

Figure 7—Iso-potential lines from a quasi-steady-state flow simulation

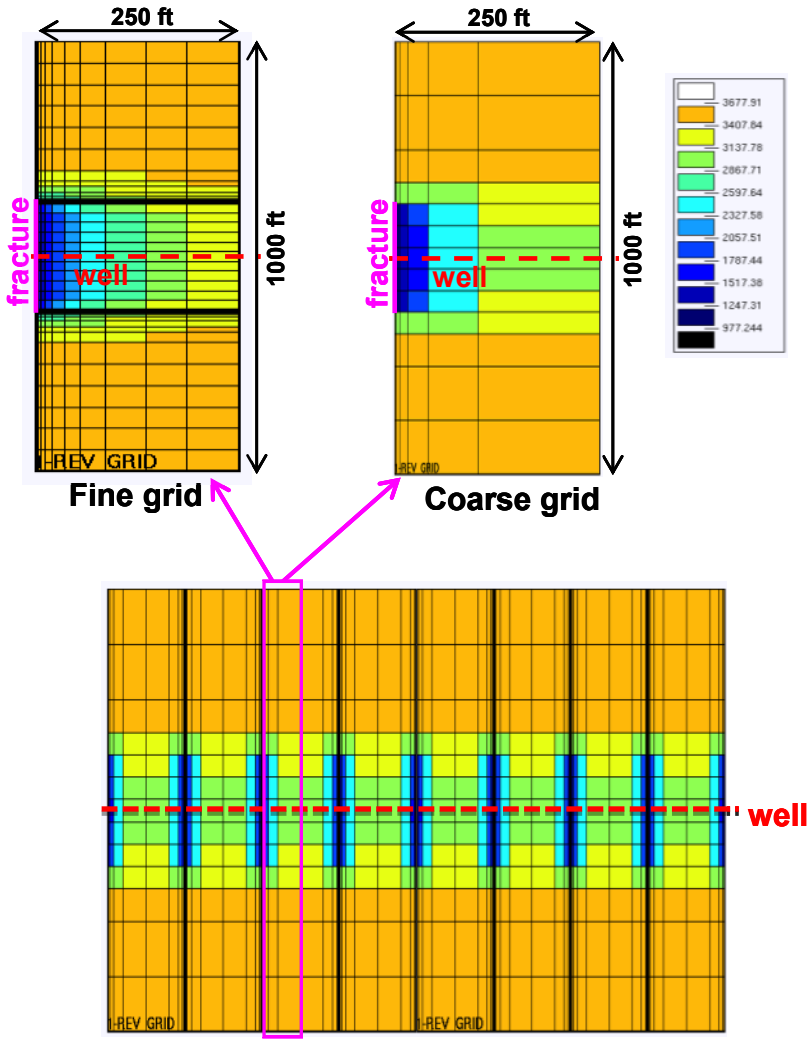

Figure 8—Simulation of hydraulic fractures in Example 1

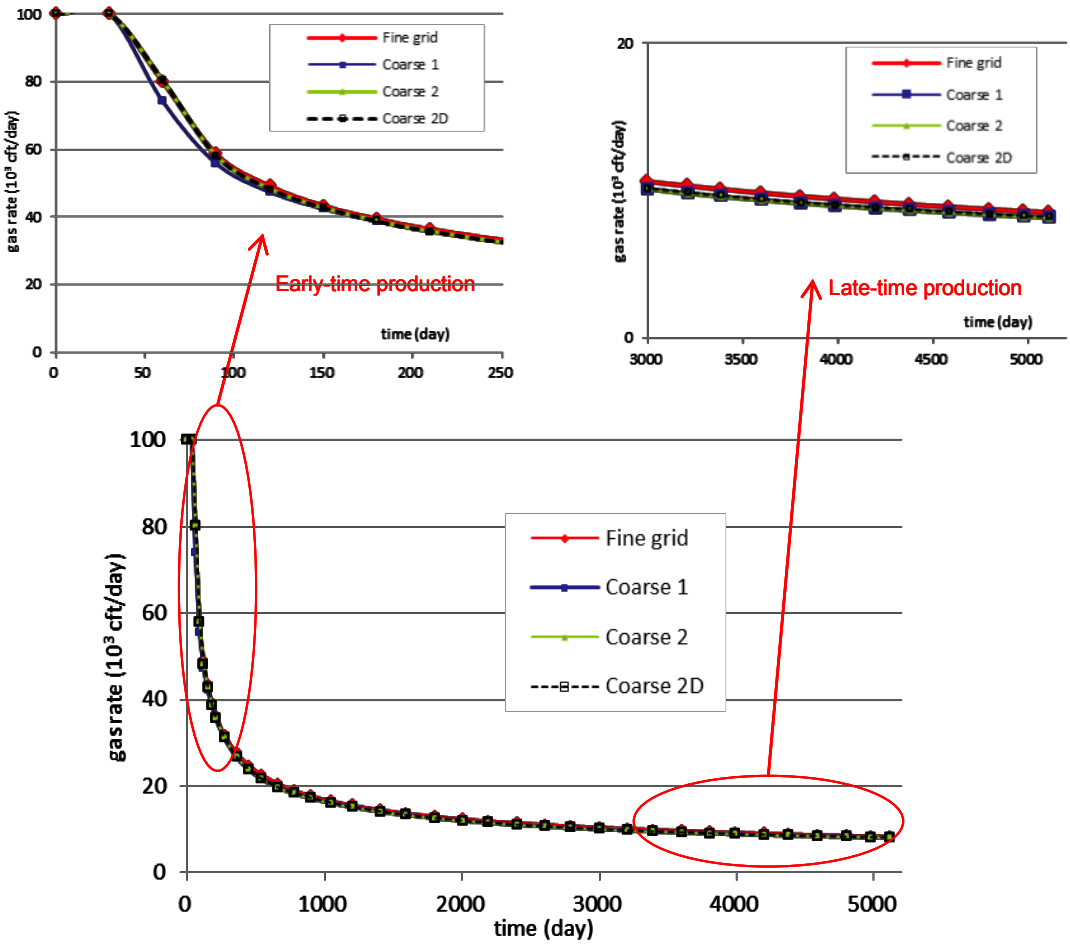

Figure 9—Gas production with different grid systems

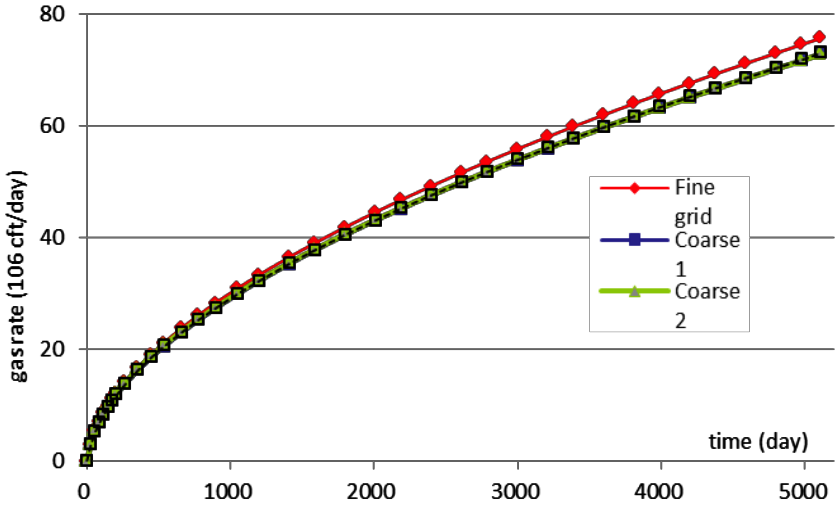

Figure 10—Cumulative gas production in the simulation of a single hydraulic fracture

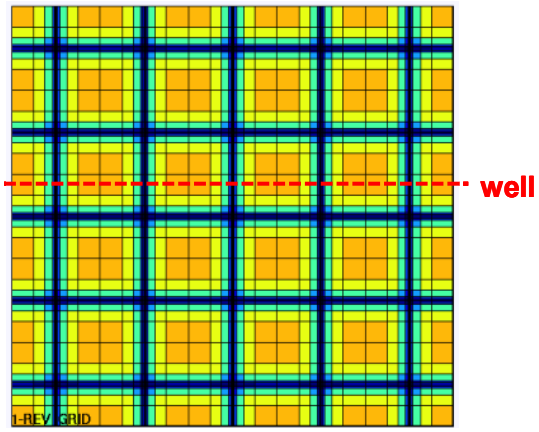

Figure 11—Simulation in a fracture network in Example 1

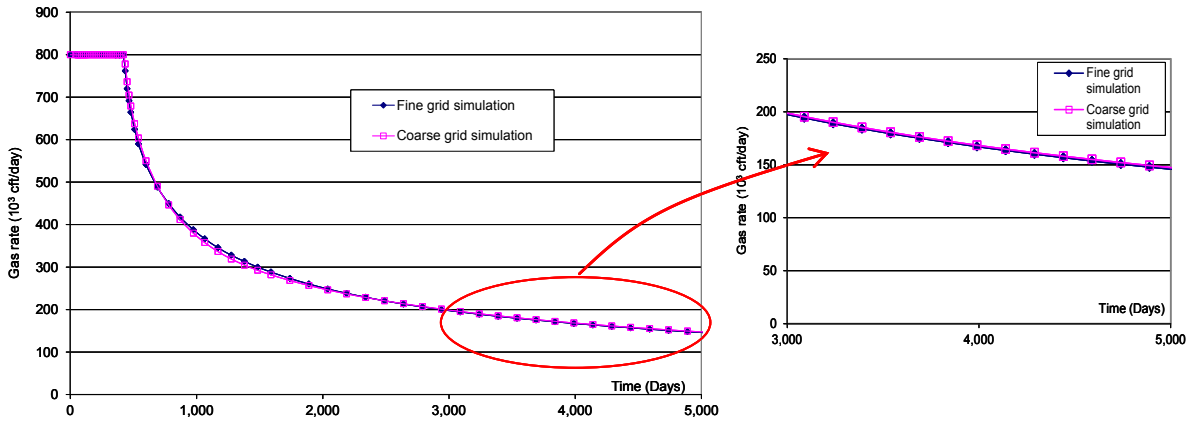

Figure 12—Gas production with fine and coarse grid simulation in the fracture network

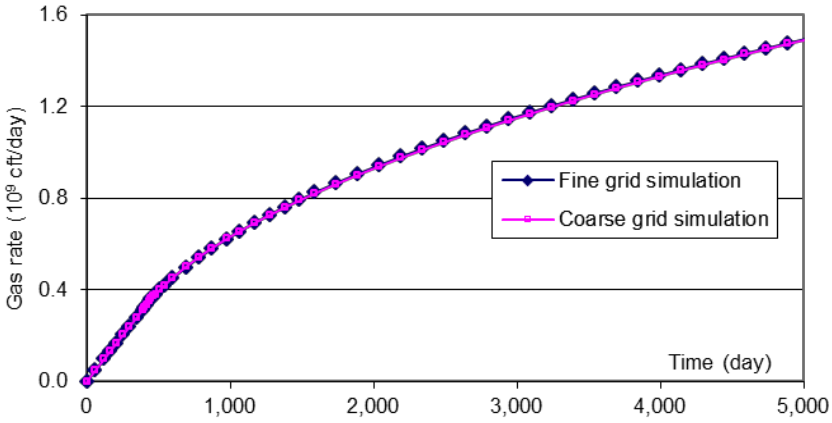

Figure 13—Cumulative gas production in the fracture network

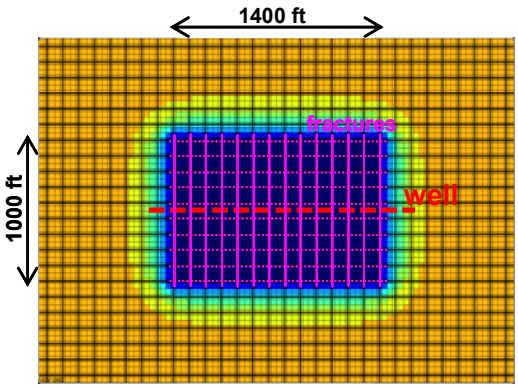

14a). Case 1 - Fracture spacing of 100 ft

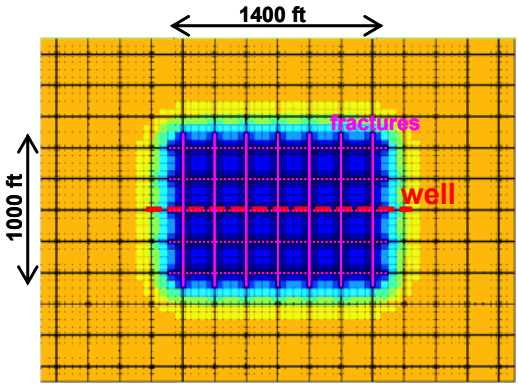

14b). Case 2 - Fracture spacing of 200 ft

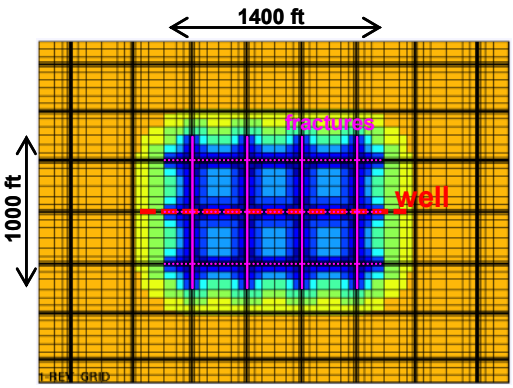

14c). Case 3 - Fracture spacing of 350 ft

Figure 14—Simulation of a multi-stage fractured horizontal well with a single-porosity model

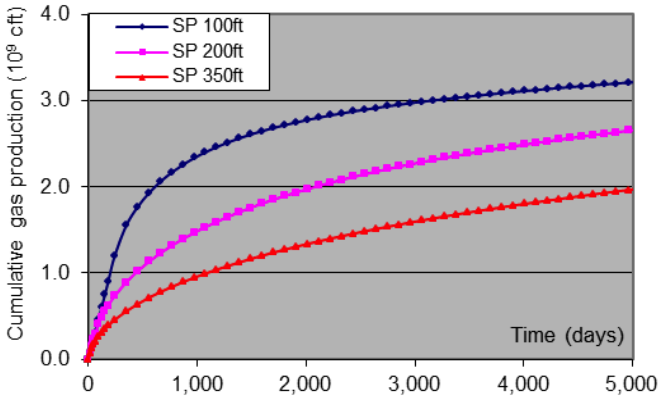

Figure 15—Comparison of single-porosity model results for different fracture spacings

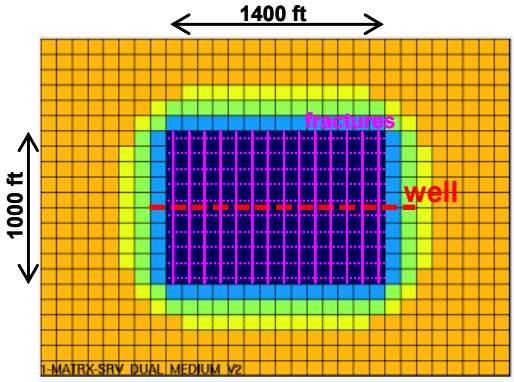

16a). Case 1 - Fracture spacing of 100 ft

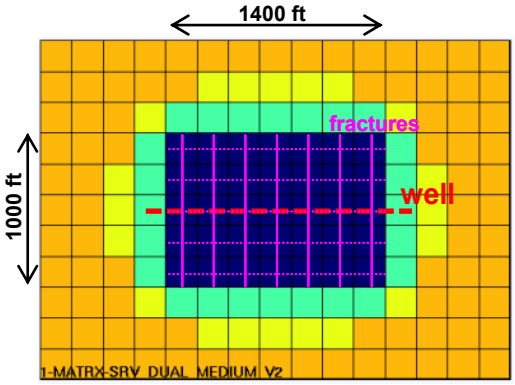

16b). Case 2 - Fracture spacing of 200 ft

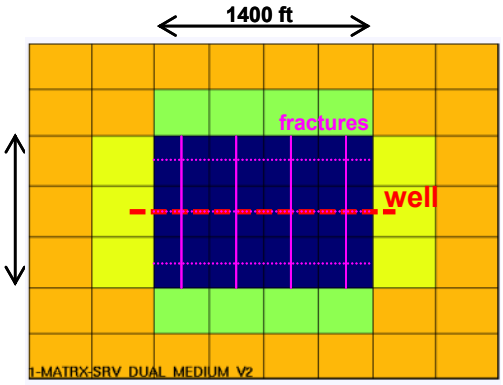

16c). Case 3 - Fracture spacing of 350 ft

Figure 16—Simulation of a multi-stage fractured horizontal well with a dual-porosity model

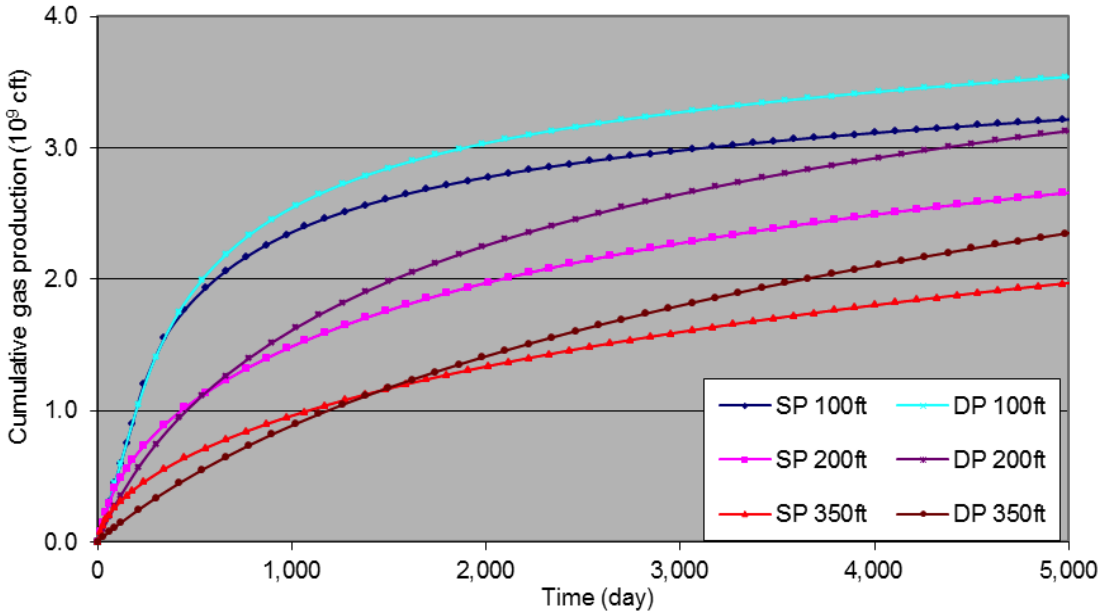

Figure 17—Simulations with a dual-porosity model

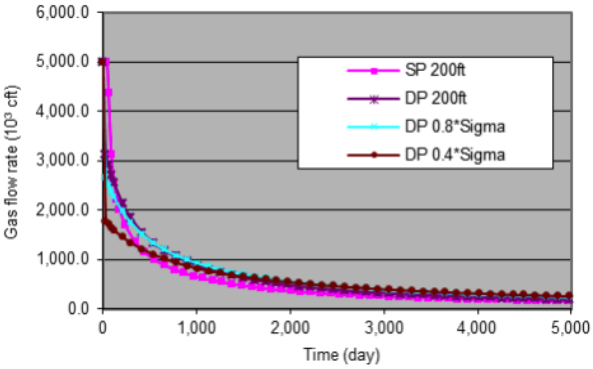

18a). Well production rate

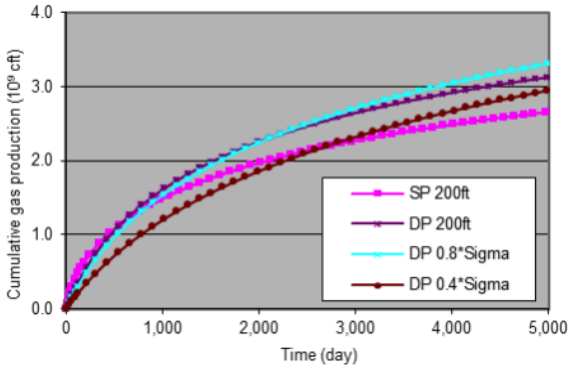

18b). Cumulative production

Figure 18—Impact of shape factor on dual-porosity model simulation

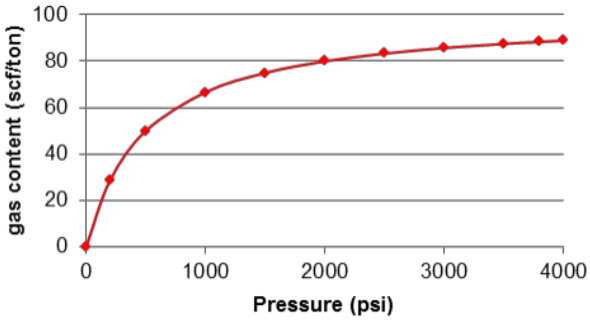

Figure 19—Adsorbed gas content

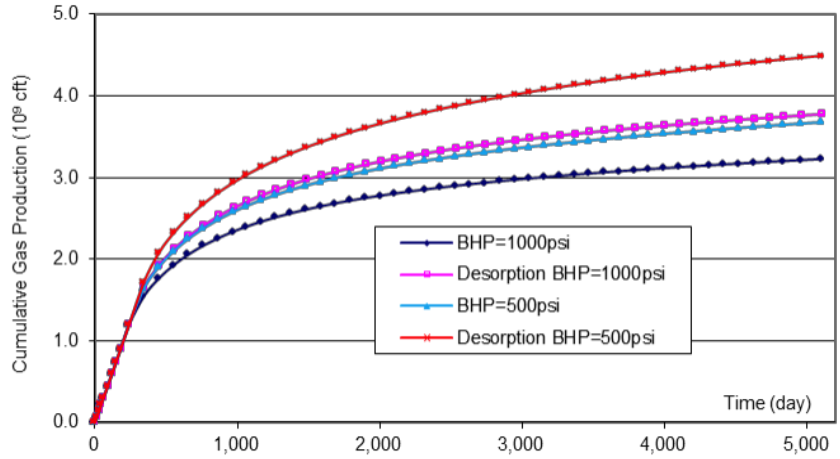

20a). Case 1: fracture spacing of 100 ft

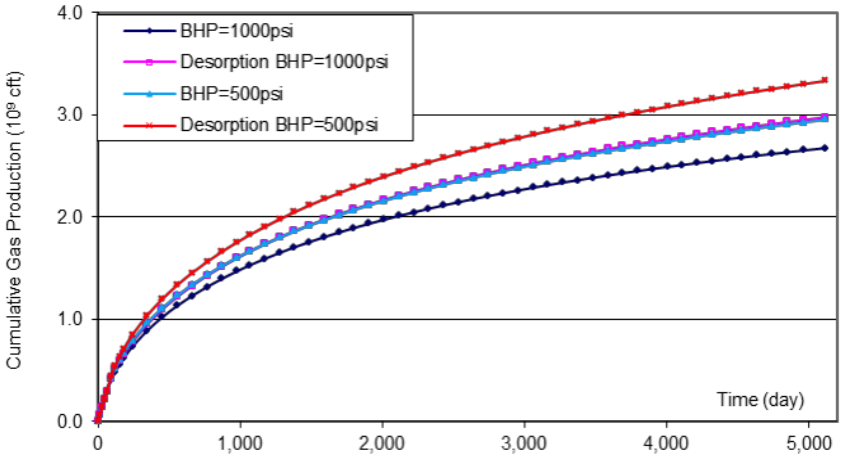

20b). Case 2: fracture spacing of 200 ft

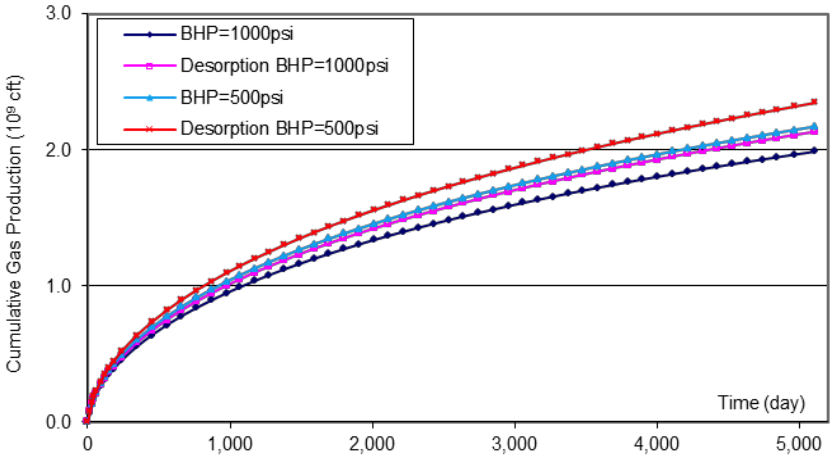

20c). Case 3: fracture spacing of 350 ft

Figure 20—Impact of gas desorption

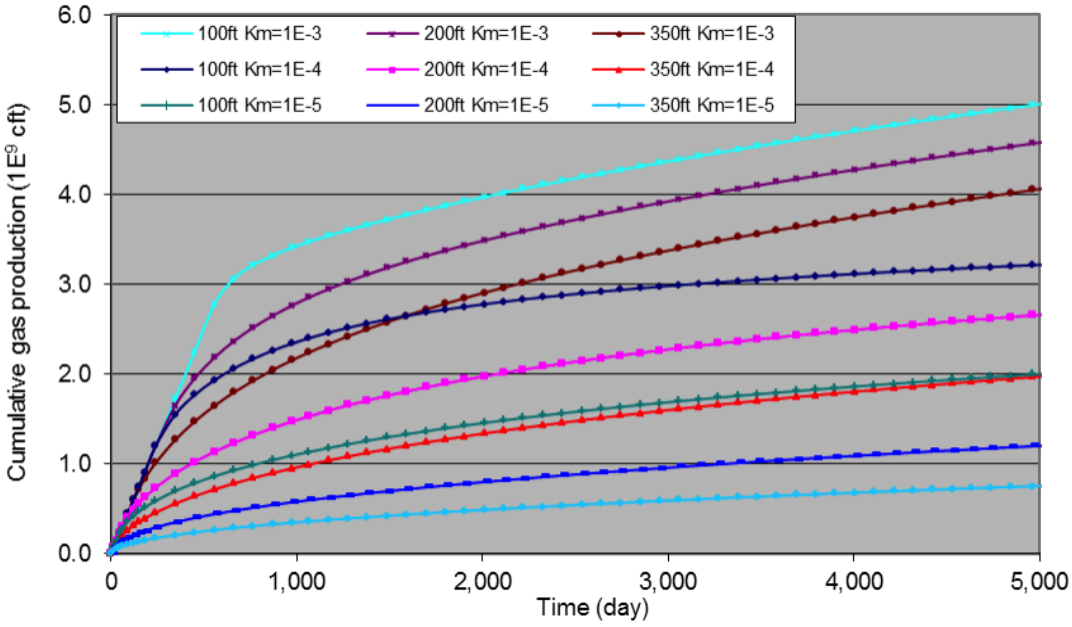

Figure 21—Impact of matrix permeability

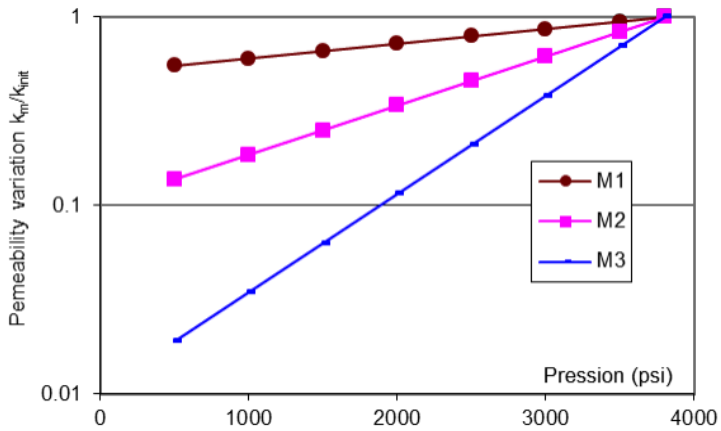

Figure 22—Permeability variation as a function of pressure

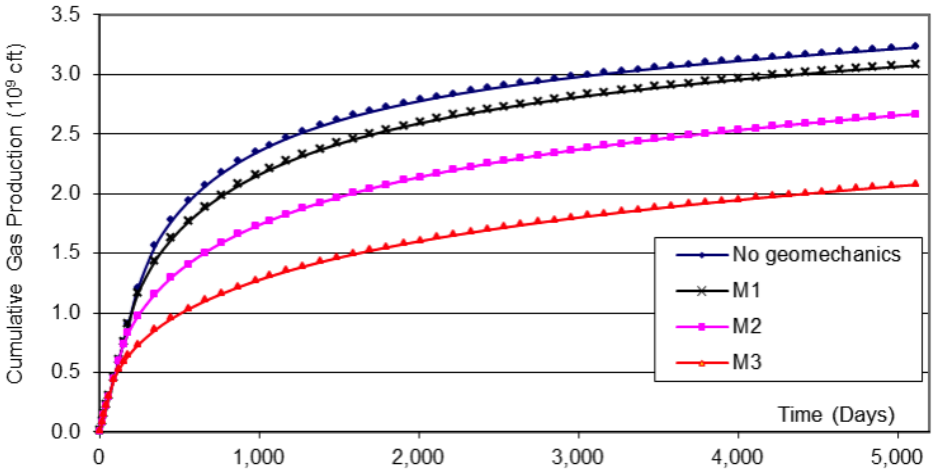

23a). Case 1: fracture spacing of 100 ft

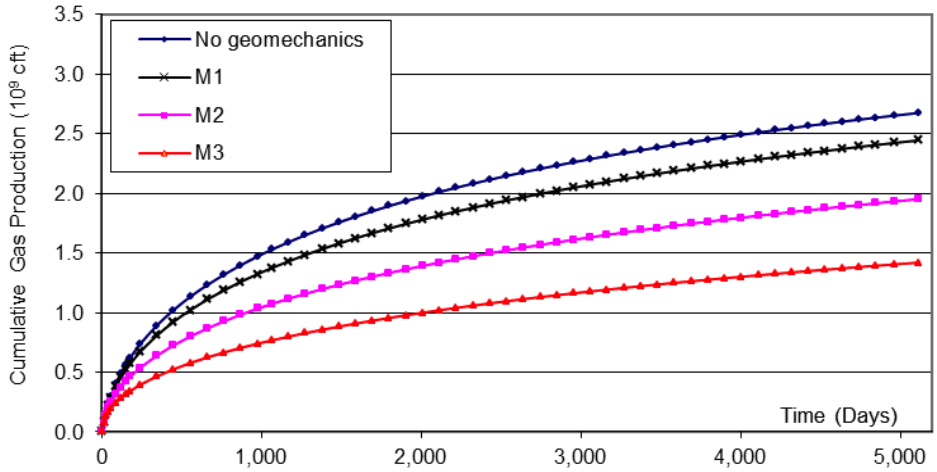

23b). Case 2: fracture spacing of 200 ft

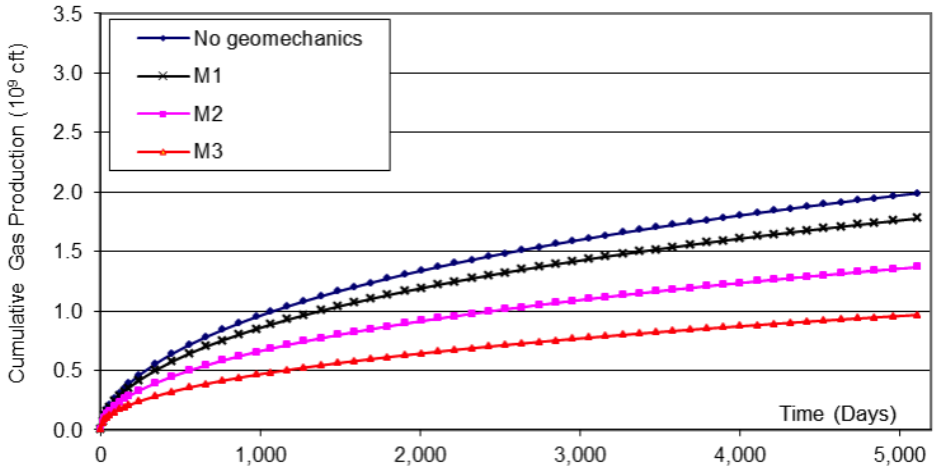

23c). Case 3: fracture spacing of 350 ft

Figure 23—Impact of geomechanics on stress sensitive shale gas reservoirs

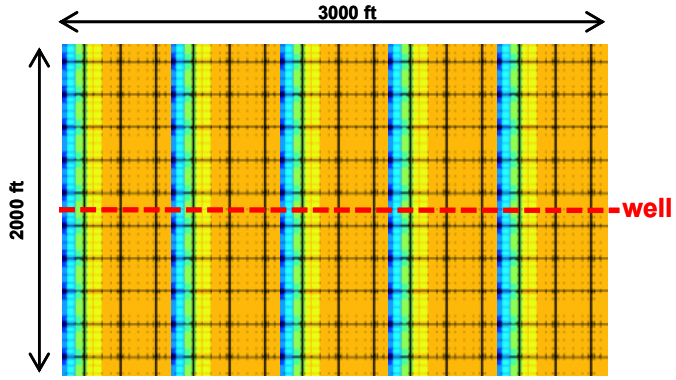

Figure 24—Simulated domain in Example 3

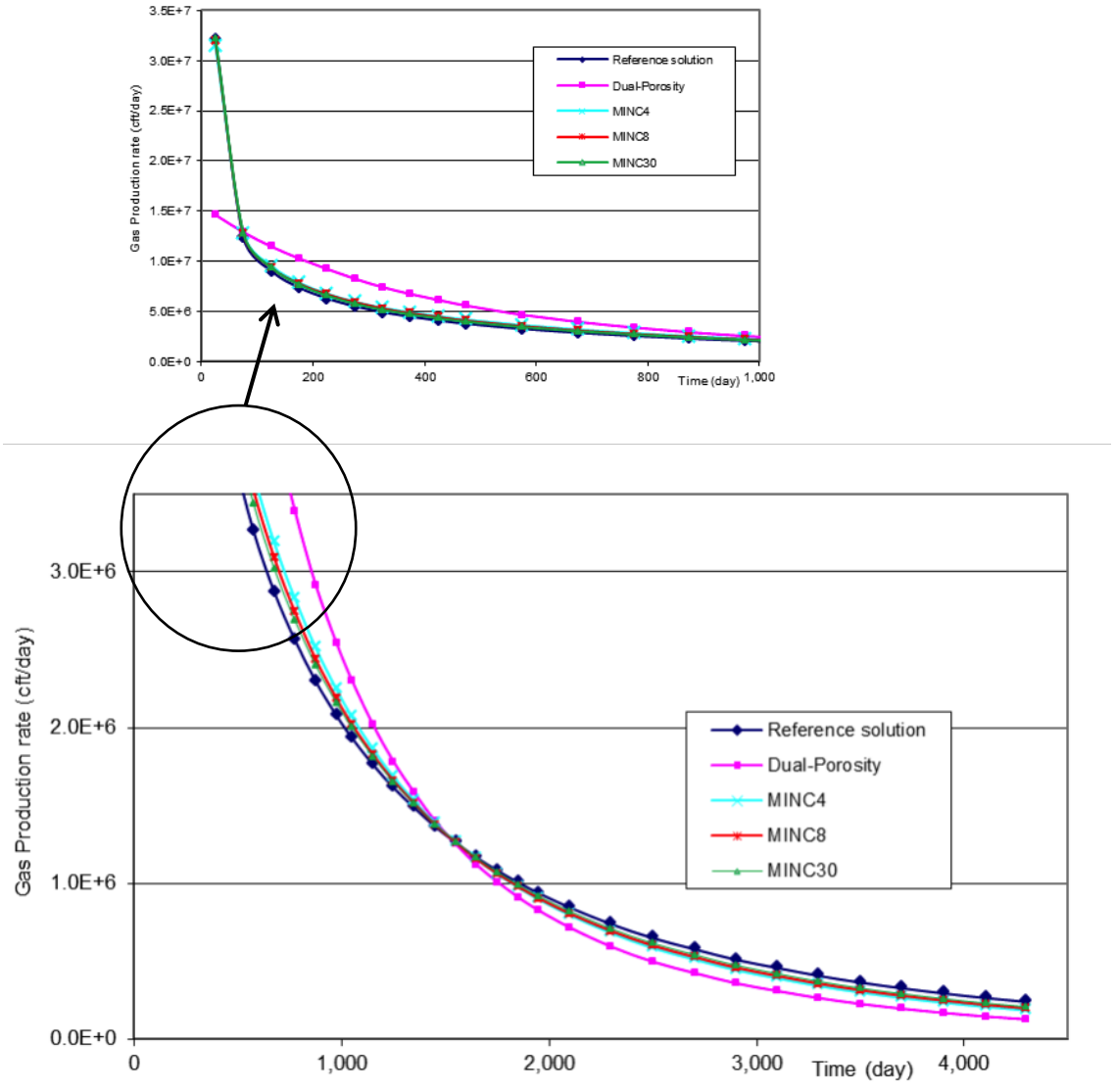

Figure 25—Gas production rate with MINC method

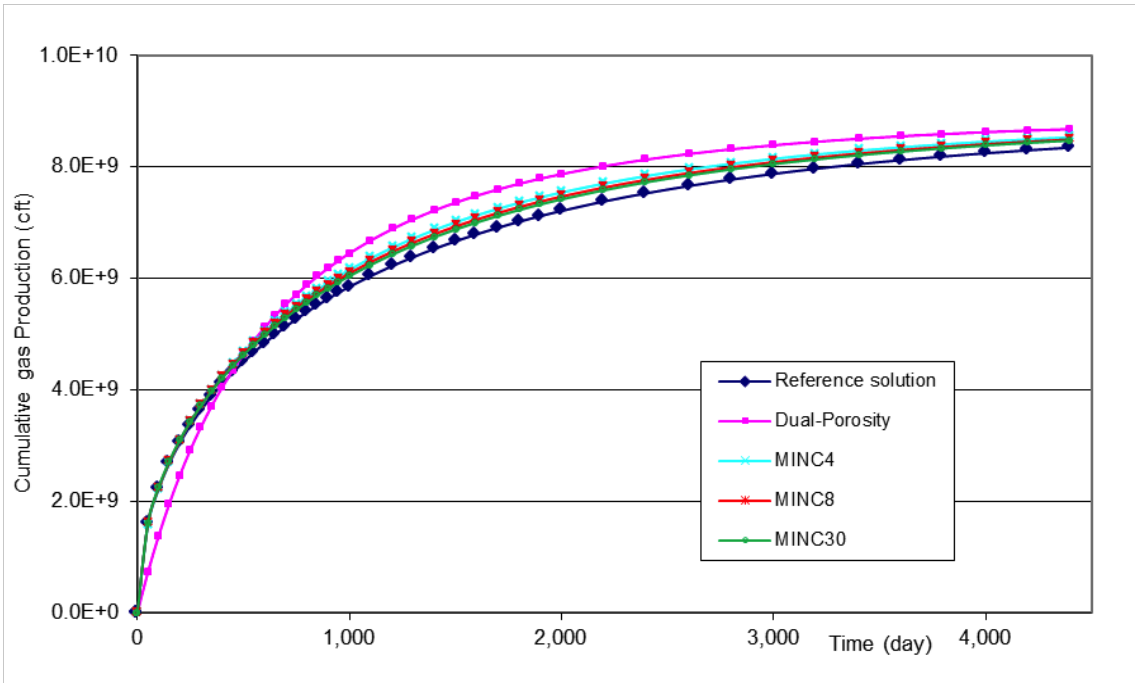

Figure 26—Cumulative production with MINC method

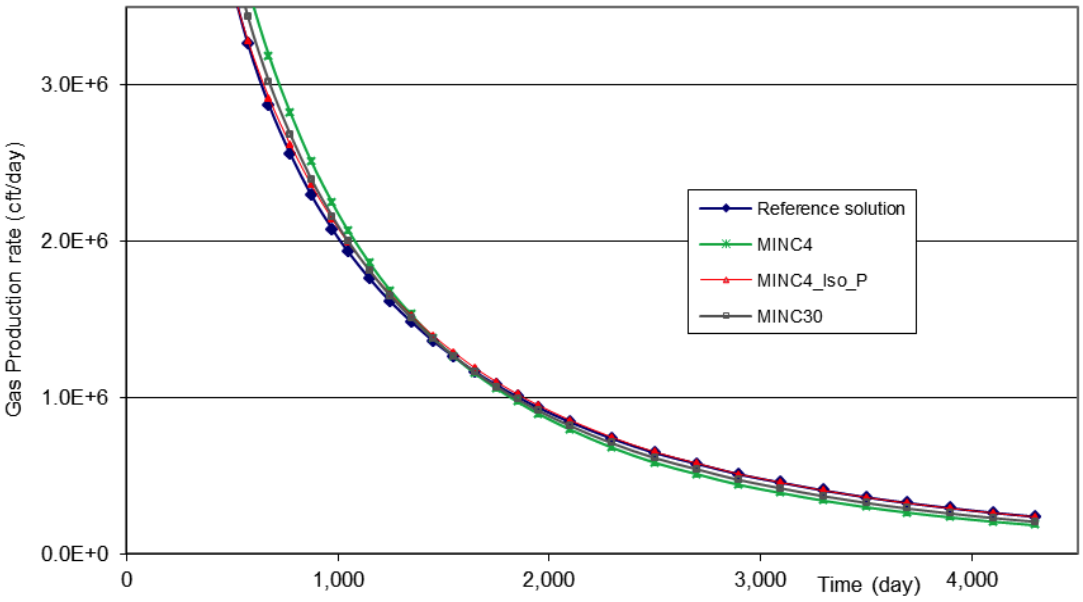

Figure 27—Improvement of MINC method on gas flow rate (4 subdivisions)

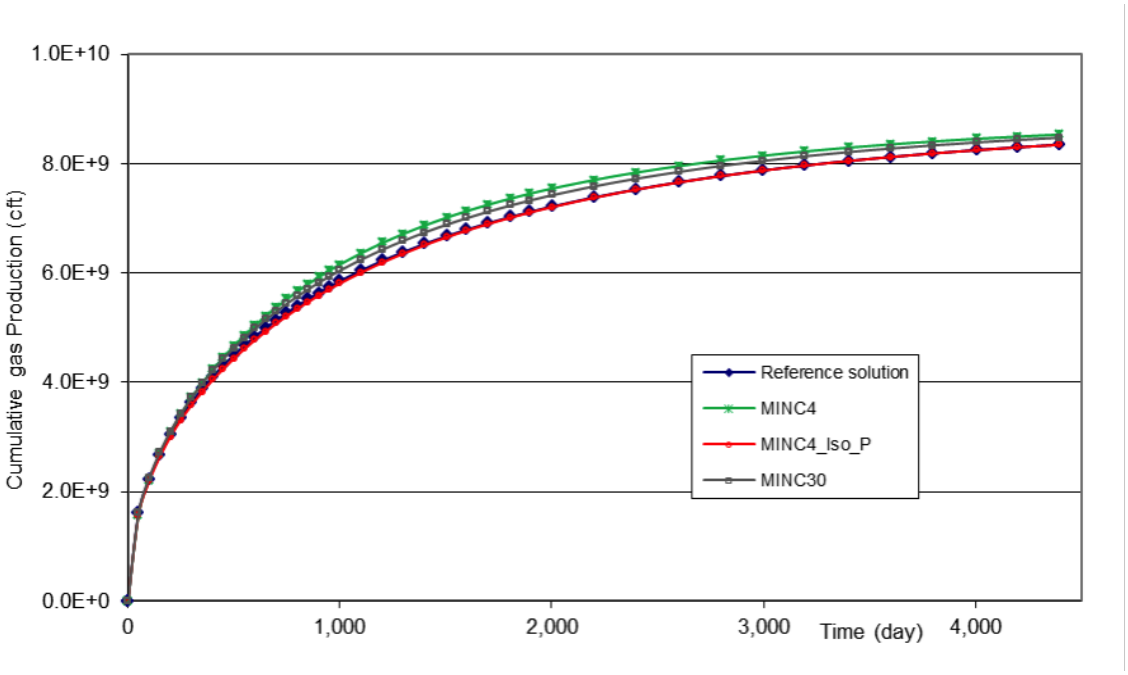

Figure 28—Improvement of MINC method on cumulative production (4 subdivisions)

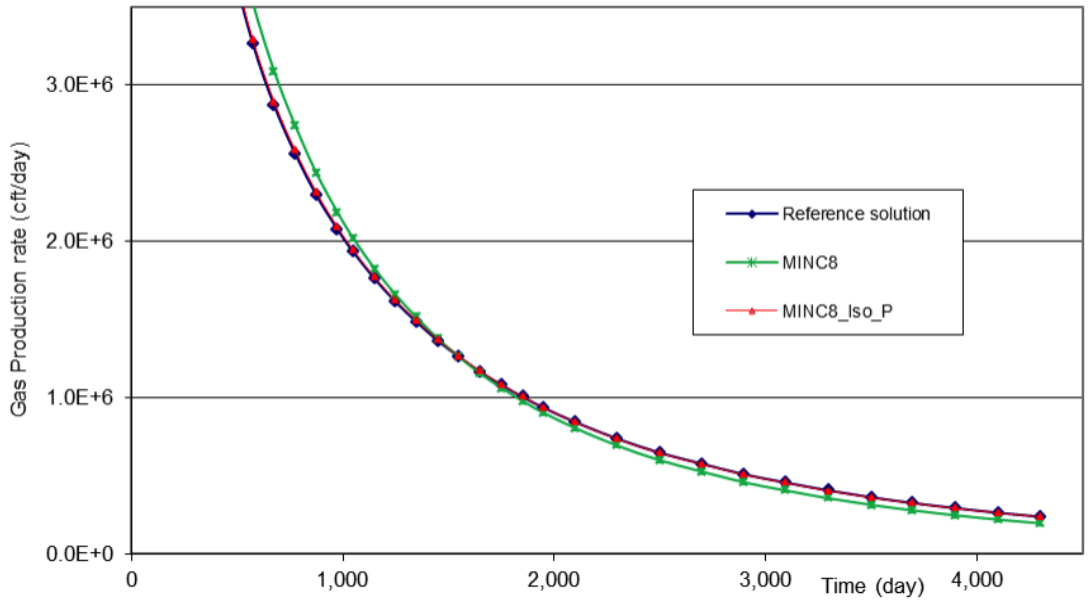

Figure 29—Improvement of MINC method on gas flow rate (8 subdivisions)

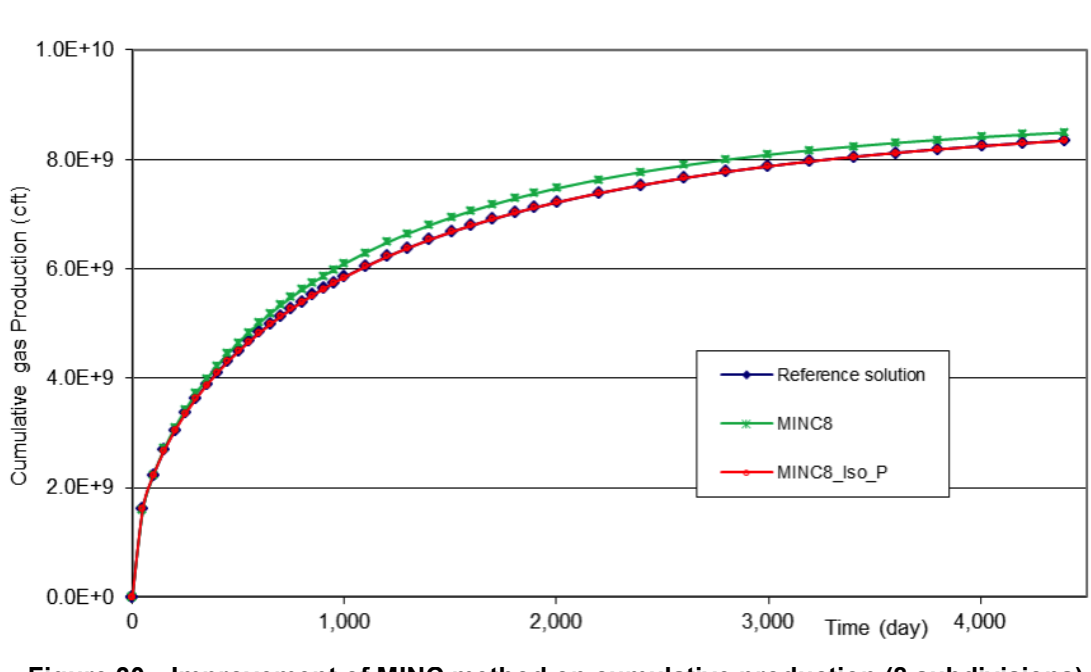

Figure 30—Improvement of MINC method on cumulative production (8 subdivisions)

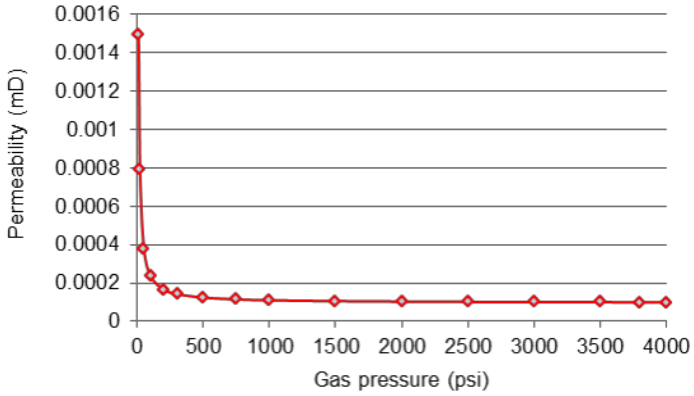

Figure 31—Gas permeability variation in tight matrix due to Klinkenberg effect

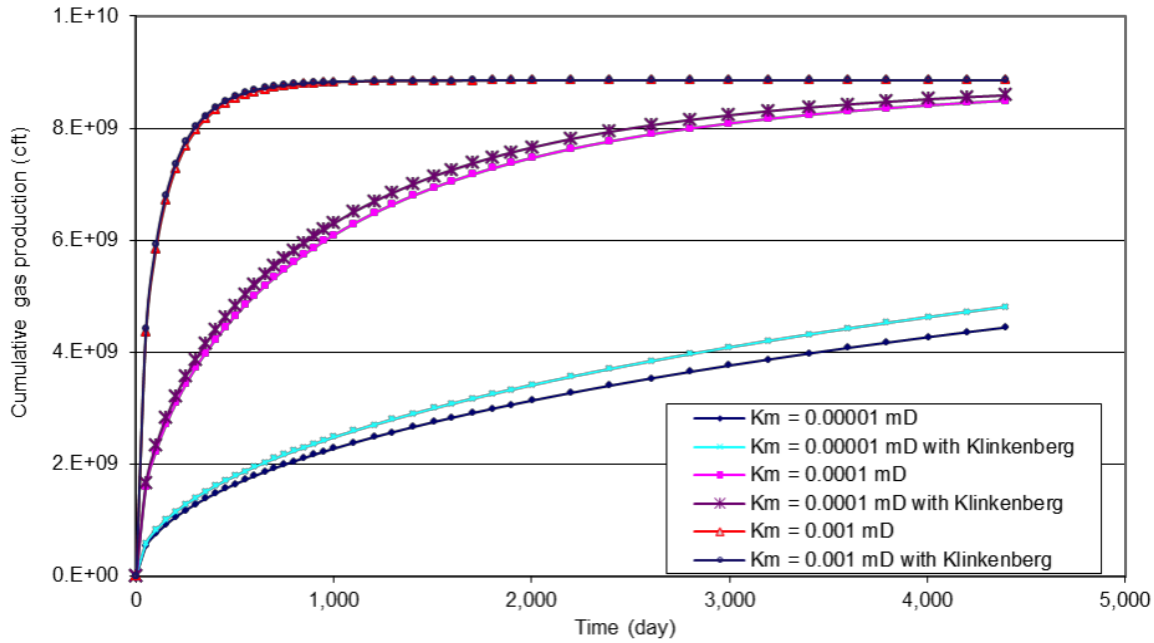

Figure 32—Klinkenberg effects

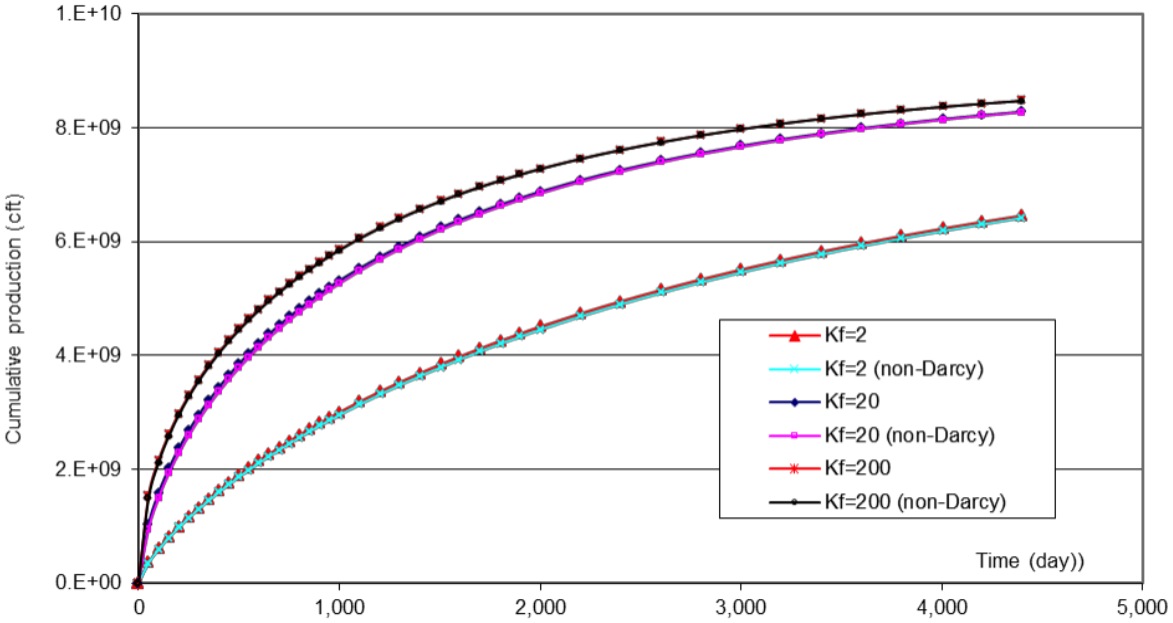

Figure 33—Non-Darcy flow effect (km = 0.0001 mD)

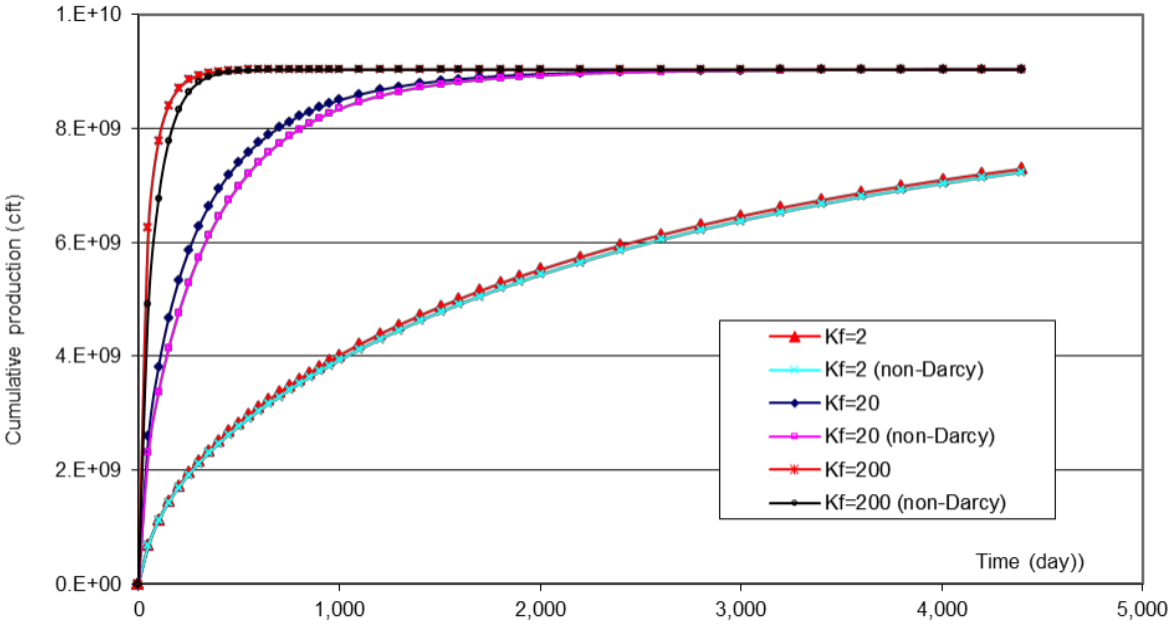

Figure 34—Non-Darcy flow effect (km = 0.01 mD)